

# Mid-Miocene to Present Upper-plate deformation of the southern Cascadia Forearc: Effects of the superposition of subduction and transform tectonics

- Kirsty A. McKenzie<sup>1\*</sup>, Kevin P. Furlong<sup>1</sup>, Eric Kirbv<sup>2</sup> 1
- 2 <sup>1</sup>Department of Geosciences, The Pennsylvania State University, University Park, PA, USA
- 3 <sup>2</sup>Department of Earth, Marine and Environmental Sciences, The University of North Carolina,
- Chapel Hill, NC, USA 4
- \* Correspondence: 5
- 6 Kirsty A. McKenzie
- kam724@psu.edu 7
- 8 Keywords: subduction<sub>1</sub>, Cascadia<sub>2</sub>, forearc<sub>3</sub>, triple junction<sub>4</sub>, tomography<sub>5</sub>, GPS<sub>6</sub>
- 9 **Abstract**
- 10 The southern Cascadia forearc undergoes a three-stage tectonic evolution, each stage involving
- 11 different combinations of tectonic drivers, that produce differences in the upper-plate deformation
- 12 style. These drivers include subduction, the northward migration of the Mendocino triple junction
- (MTJ) and associated thickening and thinning related to the Mendocino Crustal Conveyor (MCC) 13
- 14 effect, and the NNW translation of the Sierra Nevada-Great Valley (SNGV) block. We combine
- 15 geodetic data, plate reconstructions, seismic tomography and topographic observations to determine
- how the southern Cascadia upper plate is deforming in response to the combined effects of 16
- subduction and NNW-directed (MCC- and SNGV-related) tectonic processes. 17
- 18 The location of the terrane boundaries between the relatively weak Franciscan complex and the
- 19 stronger KMP and SNGV block has been a key control on the style of upper-plate deformation in the
- 20 southern Cascadia forearc since the mid-Miocene. At ~15 Ma, present-day southern Cascadia was in
- 21 central Cascadia and deformation there was principally controlled by subduction processes. Since ~5
- 22 Ma, this region of the Cascadia upper plate, where the KMP lies inboard of the Franciscan complex,
- 23 has been deforming in response to both subduction and MCC- and SNGV-related effects. GPS data
- 24 show that the KMP is currently moving to the NNW at ~8-12 mm/yr with little internal deformation,
- 25 largely in response to the northward push of the SNGV block at its southern boundary. In contrast,
- 26 the Franciscan complex is accommodating high NNW-directed and NE-directed shortening strain
- 27 produced by MCC-related shortening and subduction coupling respectively. This composite tectonic
- 28 regime can explain the style of faulting within and west of the KMP. Associated with this MCC
- 29 crustal thickening, seismic tomography imagery shows a region of low velocity material that we
- 30 interpret to represent crustal flow and injection of Franciscan crust into the KMP at intracrustal
- levels. We suggest that this MCC-related crustal flow and injection of material into the KMP is a 31
- 32 relatively young feature (post ~ 5 Ma) and is driving a rejuvenated period of rock uplift within the
- 33 KMP. This scenario provides a potential explanation for steep channels and high relief, suggestive of
- 34 rapid erosion rates within the interior of the KMP.

- 36 Upper-plate deformation in subduction zone forearcs occurs in response to both short-term
- 37 (earthquake cycle) and long-term (million-year plate interaction) processes. New observations of
- present-day and long-term upper-plate deformation along subduction zones globally allow us to 38
- 39 identify both upper-plate behavior that is common across subduction zones as well as differences in
- 40 the deformational response of the upper plate among different subduction margins. For example,
- during the 2016 Kaikoura, New Zealand event, slip on upper-plate faults was significant ( $\sim 5-10$  m) 41
- 42 and was coincident with slip on the Hikurangi subduction megathrust (Wang et al., 2018; Furlong &
- 43 Herman, 2017). Additionally there was 0.6-4.8 m of uplift of the coastline during this event (Hamling
- 44 et al., 2017). Similar upper-plate faults exist in subduction zones globally and understanding the
- 45 tectonic processes that load these faults and when they slip during the seismic cycle is important for
- 46 assessing hazard across subduction forearcs. Although the Cascadia subduction zone has not
- experienced a major megathrust earthquake in modern times, and as a result we do not have direct 47
- 48 observations of its rupture behavior, detailed recording of its current behavior by geodetic methods,
- and constraints on its plate tectonic evolution make it an ideal plate boundary to explore how plate 49
- interactions and the evolution of a plate boundary over millions of years produces permanent 50
- 51 deformation of the upper plate.
- 52 The Cascadia subduction zone extends along the western coast of North America from northern
- 53 California to British Columbia (Figure 1) and is defined by the position of the Mendocino triple
- 54 junction (MTJ) at its south end and a triple junction at its north end where the Nootka Fault Zone
- 55 (NFZ) links the northern end of the Juan de Fuca ridge to the Cascadia subduction zone (Rohr et al.,
- 56 2018). The MTJ migrates northward along the western margin of North America at approximately 50
- 57 mm/yr (Furlong and Schwartz, 2004), while the northern triple junction has been relatively stationary
- 58 with respect to North America since ~4 Ma (Rohr et al., 2018). As a result, the length of the Cascadia
- 59 subduction zone has systematically shortened over time (Figures 1 & 2). Thus, the plate tectonic
- 60 setting of our study area in southern Cascadia has significantly changed since the mid-Miocene (~15
- 61 Ma), at which time it was centrally located along the plate boundary, as compared to its current
- 62 location adjacent to the MTJ (Figure 2).
- 63 This change in the geography of southern Cascadia over the last 15 million years, and the associated
- changes in tectonic interactions in the region lead to a suite of tectonic processes (subduction and 64
- 65 transcurrent tectonics) that have contributed at different times and in different ways to upper-plate
- deformation in the region. These tectonic drivers act on a spatially varying upper-plate geology 66
- (Figure 1) resulting in distinctive styles of upper-plate deformation in both space and time. Here we 67
- 68 explore how the upper-plate geology, subduction-interface earthquake-cycle coupling, and non-
- 69 subduction tectonic processes associated with the northward encroachment of the MTJ (including the
- 70 development of the San Andreas plate boundary to the south) interact and produce the observed
- 71 upper-plate deformation in present-day southern Cascadia from the mid-Miocene to the present.
- 72 Specifically we focus on (1) how the behavior of upper-plate faults changes as the plate boundary
- 73 evolves, including the development of shear zones in the vicinity of the MTJ, and (2) the
- 74 spatiotemporal patterns of uplift across different regions of the southern Cascadia forearc, including a
- 75 possible rejuvenation in uplift of the KMP over the last 5 million years. We address these key points
- by building on our recent results delineating the kinematics and strain within the terranes in the 76
- 77 vicinity of the MTJ, including the Franciscan, Klamath, Siletz, and Sierra Nevada/Great Valley
- 78 terranes (McKenzie et al., 2022; McKenzie and Furlong, 2021). We add to those results newly
- 79 obtained crustal (local earthquake) tomography of the coastal region extending from north of the San
- 80 Francisco Bay region to approximately 42° N (Furlong et al., 2021). This tomography provides a 3-D
- image of the crustal structure of the Franciscan and Klamath terranes and defines the extent of the 81
- 82 subducting Gorda slab and the Pacific plate, south of the MTJ. We also present observations of

- 83 normalized channel steepness throughout the region, which provide additional insight into which
- regions are potentially undergoing active uplift and exhumation.

## 85 2 Background

86

## 2.1 Geologic and Tectonic Setting

- 87 The region of southern and central Cascadia from the mid-Miocene to present-day (Figures 1 & 2)
- 88 includes five key geological domains: (1) the Siletz-Crescent terrane (2) the northern California
- 89 Coast Ranges comprised largely of the Franciscan complex, (3) the Klamath Mountains province
- 90 (KMP), (4) the Great Valley Ophiolite (mafic-ultramafic body, hereinafter referred to as the Great
- Valley ultramafic body) and the Great Valley Sequence, both of which are overlain by Cenozoic
- basin fill, and (5) the Sierra Nevada (McCrory & Wilson, 2013; Schmidt & Platt, 2018; Irwin, 1985;
- 93 Godfrey et al., 1997; Ernst, 2013). North of ~43 °N, the Siletz-Crescent terrane, an accreted oceanic
- 94 plateau, makes up the majority of the forearc, inboard of the present-day offshore accretionary
- 95 margin (Figures 1 & 2) (McCrory & Wilson, 2013; Wells et al., 1998). South of ~43 °N, the upper
- 96 plate is composed of an active accretionary margin near the trench outboard of the Franciscan
- omplex, a partially exhumed relict accretionary margin, which is bounded on its east by the KMP, a
- 98 composite metamorphic/plutonic terrane (Schmidt & Platt, 2018; Irwin, 2003; Irwin, 1985). South of
- 99 the MTJ, the Franciscan complex continues as the outboard terrane, and the KMP is replaced at ~40
- °N by the Sierra Nevada Great Valley (SNGV) block composed of the accreted Great Valley
- 101 ultramafic body and the Sierra Nevada terrane.
- This variation in upper-plate geology and the interaction among the geologic terranes plays an
- important role in the style and evolution of upper-plate deformation along the western margin of
- North America, which can be divided into three stages, each reflecting differences in the principal
- tectonic drivers acting during each time period (Figure 2, 3).
- 106 Stage 1: When the MTJ is sufficiently south of a site, corresponding currently to the region of
- 107 Cascadia north of ~43 °N, the primary tectonic driver of upper-plate deformation is subduction plate
- interface coupling.
- 109 Stage 2: As the MTJ migrates northward and approaches the region of interest, NNW-directed
- shortening associated with the motions of the MTJ and SNGV block is superimposed on the
- subduction coupling signal, producing a composite deformation field.
- 112 Stage 3: After the MTJ passes, a slab window is created beneath the upper-plate region that
- experienced the previous subduction and MTJ/SNGV-related deformation. This relic upper-plate
- region of southern Cascadia now responds to deformation primarily within the Pacific North
- America shear zone. Localization of shear and fault development within this zone leads to the
- development of the San Andreas plate boundary, and upper-plate deformation is overprinted on the
- inherited (pre-MTJ passage) structures from the prior tectonic regime.
- The evolution of the plate boundaries among the Pacific, North America, and Juan de Fuca (Gorda)
- plates along the western margin of North America results in fundamental changes in plate
- interactions over millions of years. For example, the MTJ, which defines the transition from
- subduction to translation has migrated nearly 500 km northward, relative to North America since ~10
- Ma (Atwater, 1970) (Figures 2 & 3). This means that the current San Andreas plate boundary zone
- 123 (Pacific North America) north of San Francisco was part of the Cascadia subduction zone as
- recently as 5-10 million years ago, with the SNGV block being the main upper-plate terrane inboard

- of the Franciscan complex. The San Andreas plate boundary faults have subsequently developed
- within a deformed upper-plate that has undergone both subduction deformation and subduction/MTJ-
- 127 SNGV composite deformation prior to the passage of the MTJ.

## 2.2 Development of the Present-Day Tectonic Setting

128

144

- The lithospheric-scale geometry of the plate boundary in the vicinity of the MTJ results from the way
- in which the plate boundary changed from subduction to a system with northward and southward
- migrating triple junctions and the development of a transform plate boundary (Figure 3). Based on
- plate reconstructions the initial triple junctions formed with the interaction of a short ridge segment,
- bounded on its north by the intersection of the Pioneer fault with the North American margin (Figure
- 3(a),(b)) (Furlong et al., 2003; Atwater, 1970). The resulting northward-migrating Pioneer triple
- junction (PTJ) was a short-lived configuration, and within a few million years the Mendocino fault -
- ridge intersection reached the trench producing the MTJ (Figure 3(c)) As a result, the PTJ was
- abandoned and the short ridge segment linking the Pioneer and Mendocino faults ceased spreading.
- The fragment of the Farallon plate between the two triple junctions (PTJ and MTJ), the Pioneer
- fragment, was captured by the Pacific plate, and has traversed the North American margin with the
- Pacific plate since ~ 25 Ma as the MTJ migrates northward (Figure 2(c)) (Furlong et al., 2003). This
- fragment extends some distance under the western edge of North America, which results in the slab
- window, just to the south of the MTJ, to be narrower than might otherwise be expected, based on the
- subduction geometry north of the MTJ (Figure 3(d)).

### 2.3 Deformational Effects of Present-Day Tectonics in Southern Cascadia

- 145 Present-day deformation in the southern Cascadia forearc is governed by the interaction of three
- tectonic plates, the Pacific plate, the Juan de Fuca (Gorda) plate and the North American plate, that
- meet at the MTJ. With the passage of the MTJ, a slab window is created in the wake of the
- subducting slab (Furlong, 1984; Zandt & Furlong, 1982; Dickinson & Snyder, 1979). Furlong &
- Govers (1999) proposed that associated with the creation of this slab window, asthenospheric mantle
- will flow into the region and viscously couple the North American plate above to the adjacent
- southern edge of the subducting Gorda slab. This emplacement of asthenosphere into the slab
- window and associated viscous coupling (via the Mendocino Crustal Conveyor (MCC) model) drives
- a northward motion of the overriding North American plate in the vicinity of the MTJ, leading to
- 154 crustal shortening and thickening ahead of the MTJ and crustal thinning in its wake (Furlong &
- 155 Govers, 1999). This wave of crustal thickening and thinning propagates to the NNW at ~50 mm/yr
- with the MTJ. Associated with this northward migration are variations in crustal structure,
- uplift/subsidence, river drainage reorganization and thermal variations within this MCC deformation
- 158 corridor (Bennett et al., 2016; Lock et al., 2006; Furlong & Schwartz, 2004; Guzofski & Furlong,
- 159 2002; Beaudoin et al., 1996, 1998). This deformation associated with the MCC (long-term NNW-
- oriented geologic shortening followed by extension) is superimposed in the existing subduction-
- driven deformational field as the MTJ approaches.
- At present, in the region south of the MTJ, Pacific-North America right-lateral shear motion is
- accommodated in two shear zones. Approximately 75 % of the motion is accommodated within the
- 164 coastal region, extending to the western edge of the Great Valley (Bennett et al., 1999, 2003). An
- additional 25 % of this motion is accommodated inboard of the main plate boundary along the
- eastern margin of the SNGV crustal block (Bennett et al., 1999, 2003), in what is termed the Eastern
- 167 California Shear Zone (ECSZ). This inboard shear initiated at ~12-10 Ma, causing a change in the
- direction of the SNGV motion from westward to north-northwestward (McQuarrie & Wernicke,
- 169 2005). This north-northwestward motion along the northern ECSZ, and therefore motion of the

- 170 SNGV block, accelerated at ~ 6 Ma due to the northward motion of Baja California (Plattner et al.,
- 171 2010). Taken together, this combination of tectonic processes means that present-day upper-plate
- deformation in southern Cascadia records the superposition of processes including Cascadia 172
- 173 subduction earthquake cycle deformation, the migration of the MTJ and its associated thickening-
- 174 thinning effects, and the NNW motion of the SNGV block facilitated by shear across the northern
- ECSZ (Figures 1 & 4; McKenzie et al., 2022; McKenzie & Furlong, 2021). 175
- 176 Over the past several million years, the upper-plate region of the southern Cascadia subduction zone
- 177 has undergone a transition from a subduction-only tectonic regime to a setting in which the
- 178 subduction environment is becoming increasingly overprinted by deformation associated with the
- 179 advancing MTJ and the SNGV block (Figures 2, 3, 4). The combination of time-varying tectonic
- 180 drivers and heterogeneous upper-plate crustal properties produces a resulting deformation field that
- 181 we are able to dissect in order to explore how these events and processes combine to produce the
- 182 resulting geological signature of upper-plate deformation. Among the processes we identify are the
- 183 localization of upper-plate shortening, active rock uplift and the development of shear zones.

#### 3 The Kinematic Evolution of Southern Cascadia

184

- 185 The superposition of subduction-related and NNW-directed (MTJ and SNGV) deformation can be
- 186 seen in the GPS velocity field in southern Cascadia – documented by McKenzie & Furlong (2021)
- 187 (Figure 4, Figure S1). The subduction component is driven by the earthquake cycle and so it
- 188 accumulates and recovers every few hundred years during megathrust events. In contrast, the MCC-
- 189 and SNGV-driven components have a characteristic time scale of a few million years and their
- 190 effects are long-lived or permanent (McKenzie & Furlong, 2021; Furlong & Govers, 1999). Thus
- 191 following a large megathrust earthquake, the effects of subduction zone inter-seismic loading of the
- 192 upper plate would be largely recovered, and the residual GPS velocity field would predominantly
- 193 reflect upper-plate deformation in response to the NNW-directed components.
- 194 The present-day GPS velocity field has alternatively been interpreted to reflect rotation of rigid
- crustal blocks superposed on subduction (McCaffrey et al., 2000, 2007, 2013; Savage et al., 2000, 195
- 196 Figure 4(a)). One suggested driver for this inferred forearc rotation is the NNW-migration of the
- 197 Sierra Nevada - Great Valley (SNGV) block, which currently moves with respect to North America
- 198 at approximately 11-13 mm/yr (Plattner et al., 2010; Dixon et al., 2000; Argus and Gordon, 1991). In
- 199 that scenario, the SNGV block would impose a NNW-directed force along the southern edge of the
- 200 forearc causing blocks to rotate clockwise (McCaffrey et al., 2007). The motion of the SNGV is
- 201 similar to the displacements produced by the MCC, so the two processes could combine to enhance
- 202 the NNW-directed effects on the observed GPS velocity fields (McKenzie and Furlong, 2021). Since
- 203 the SNGV block and the MTJ are moving northward at 11-13 mm/yr and 50 mm/yr respectively,
- 204 their combined effect on the velocity field of southern Cascadia would have been significantly
- 205 different in the past. In our analyses we use the results of McKenzie and Furlong (2021), in which
- 206 they use plate reconstructions to incorporate the migrating effects of the tectonic processes that act in
- 207 southern Cascadia. We show the 9 Ma, 5 Ma, and present-day kinematics of the study region using
- these plate reconstructions and estimate the GPS equivalent velocity field pattern (termed here 208
- 209 synthetic paleo-GPS) over these times intervals in light of the past plate motions and the locations of
- 210 the MTJ and SNGV block (Figure 4). We then decompose the present-day GPS velocity field into a
- 211 subduction coupling and a NNW-directed component to investigate how strain related to subduction
- 212 coupling, the MCC and the SNGV block motion is distributed across the southern Cascadia upper-
- 213 plate. The decomposed present-day velocity fields for the full extent of the Cascadia subduction zone
- 214 are shown in Figure S1, and the decomposed data are in Table S1. These results place constraints on

- 215 where shortening strains are highest, where we would expect high uplift rates, and where shear zones
- are developing at present in southern Cascadia. 216

#### **Kinematic Reconstruction**

217

247

255

- 218 The plate kinematics for the study region at ~9 Ma, ~5 Ma and the present are shown in Figure 4.
- 219 The synthetic paleo-GPS in Figures 4(a) and 4(b) indicate that the MCC and the motion of the SNGV
- 220 block only started to affect the upper-plate kinematics of the present-day region of southern Cascadia
- 221 at  $\sim$ 5 Ma (Figure 4). The  $\sim$ 9 Ma reconstruction (Figure 4(a)) shows that the region of present-day
- 222 southern Cascadia at ~9 Ma would be centrally located along the Cascadia margin and would have
- 223 primarily been deforming as a consequence of subduction coupling processes. At this time the MTJ
- 224 was significantly further south than it is today and so the effects of the MCC processes would not
- 225 have reached this region. Additionally, at ~9 Ma the SNGV block was ~100 km south of its current
- 226 location and had not yet started moving northward in response to motion across the northern ECSZ
- 227 (Plattner et al., 2010). Also, southern Cascadia at ~9 Ma (38 °N - 40 °N, i.e. the region now south of
- the present-day MTJ) would be deforming in response to subduction coupling and the shortening 228
- 229 effects of the MCC, but unlike today the SNGV would not have been a key driver of upper-plate
- 230 deformation in the region. The apparent clockwise rotation seen today in south-central Cascadia
- 231 would be muted, with the NNW-directed velocity field decaying rapidly inland. In addition, at this
- 232 time (~9 Ma), there would have been a significant space between the northern end of the present-day
- 233 surface expression of the SNGV block and the southern margin of the KMP. The two terranes are
- 234 currently adjacent, suggesting the material in this gap has either shortened and led to crustal
- 235 thickening or underthrust the KMP. Seismicity and several east and northeast-oriented faults and
- 236 folds in the northernmost region of the Great Valley and surrounding regions are indicative of north-
- 237 south/northwest-southeast shortening between the Great Valley block and KMP (Angster et al., 2020;
- Unruh & Humphrey, 2017; Unruh et al., 2003), suggesting that at least some of this gap-closure is 238
- 239 accommodated by upper-plate shortening.
- 240 From ~5 Ma, the present-day region of southern Cascadia may have started to display the apparent
- rotation that we see in the GPS velocities today (Figure 4(b)), in response to the MTJ northward 241
- 242 migration and the onset of SNGV-related deformation. Figure 4 highlights that over the past ~10
- 243 million years, the key drivers of deformation in present-day southern Cascadia and south of the MTJ
- 244 have changed, and it is only recently (since ~5 Ma) that the present-day southern Cascadia upper
- 245 plate, including the KMP, has been deforming in a composite tectonic regime with subduction, MCC
- 246 and SNGV deformational drivers.

### Present-day tectonic components of the Cascadia GPS velocity field

- 248 We separate the present-day GPS velocity field into two components, a NE-oriented
- 249 subduction-coupling driven component and a NNW-oriented component reflecting displacements
- associated with the northward motion of the MTJ and SNGV block (McKenzie & Furlong, 2021). 250
- 251 From these two displacement components we find that both the NE-directed and NNW-directed
- 252 shortening strain rates are highest within the Franciscan complex, to the west of the KMP. The KMP
- itself is accommodating very low NE- and NNW-oriented shortening rates of ~10<sup>-16</sup> s<sup>-1</sup> (McKenzie et 253
- 254 al., 2022; McKenzie & Furlong, 2021).

#### 3.2.1 NNW-directed deformation

- 256 The NNW-directed GPS velocity field shows a steep decreasing gradient in velocities over a distance
- of  $\sim 40\text{-}50 \text{ km}$  (shortening strain rate of  $\sim 10^{-14} \text{ s}^{-1}$ ) north of the MTJ within a relatively narrow 257

- 258 channel between the subduction trench to the west and the KMP to the east (Figure 5(a)). This has
- 259 been interpreted to reflect crustal shortening associated with the MCC process (McKenzie & Furlong,
- 2021; Furlong & Govers, 1999). In contrast, to the east of the MCC corridor, the NNW-directed 260
- 261 velocity field has a shallow decay from ~12 mm/yr to 8 mm/yr from south to north across the KMP
- (shortening rate of  $\sim 10^{-16}$  s<sup>-1</sup>). Although the KMP is internally experiencing low shortening rates, the 262
- northwestern-most region of the KMP (north of the Cave Junction fault, a structure inferred to mark 263
- 264 the mountain front near Cave Junction, Oregon (Kirby et al., 2020, 2021; Von Dassow & Kirby,
- 2017) is currently undergoing crustal shortening at strain rates of ~10<sup>-15</sup> s<sup>-1</sup> (Figure 5(b)). This NW 265
- region of the KMP, a portion of the Siskiyou Mountains, exhibits relatively high topographic relief 266
- 267 compared to its surroundings, and the association of high relief, steep channels and elevated erosion
- 268 rates (e.g. Balco et al., 2013) suggest that this relief may be relatively young (McKenzie & Furlong,
- 269 2021, Kirby et al., 2020, 2021). We infer that the northward velocity gradient represents the
- 270 relatively rigid motion of the KMP in response to the northward motion of the SNGV-block to its
- 271 south – pushing on the southern margin of the KMP and, in turn, causing the KMP to impinge on the
- 272 region of the Siskiyou Mountains (McKenzie & Furlong, 2021). This push on the southern margin of
- 273 the KMP, leads the KMP to move relatively rigidly to the NNW with respect to North America.
- 274 In addition to NNW-directed shortening, we observe right-lateral differential motion between the
- 275 Franciscan crust within the MCC corridor and the KMP (Figure 5(c)). This differential motion
- 276 implies a narrow zone of NNW-oriented right lateral shear adjacent to the KMP's western boundary.
- 277 This localized region of right-lateral shear spatially coincides with a zone of upper-plate forearc
- 278 translational faults inboard of a zone of forearc compression (Kelsey & Carver, 1988). The zone of
- 279 forearc translation contains several NNW-oriented faults including the Grogan fault, the Lost Man
- 280 fault and the Bald Mountain fault zone to the north, and the Eaton Roughs and Lake Mountain fault
- 281 zones further south (Kelsey & Carver, 1988; Figure 1). These faults are optimally oriented for NNW-
- 282 oriented right-lateral shear produced by MCC- and SNGV-driven components.

### 3.2.2 Subduction Earthquake Cycle Deformation

- 284 The NE-component of the GPS velocity field reflects how the upper plate is being deformed in
- 285 response to subduction plate interface coupling along the Cascadia margin. Similar to the NNW-
- 286 component, the subduction component of the GPS velocity field shows a localized region of
- shortening within the Franciscan complex, west of the KMP. This is characterized by a steep gradient 287
- 288 in the NE-directed surface velocities from ~17 mm/yr to ~5 mm/yr over a distance of ~125 km within
- the Franciscan complex a shortening strain rate of  $\sim 10^{-15}$  s<sup>-1</sup> (Figure 6). East of the Franciscan 289
- 290 complex within the KMP, the NE-directed GPS velocities remain at ~5 mm/yr across the region
- 291 (Figure 6). This localization of shortening within the weak Franciscan material can be linked to the
- 292 effects of subduction mechanical locking terminating within the relatively weak crustal domain (the
- 293 Franciscan complex) to the west of a rigid backstop - the KMP (McKenzie et al., 2022). In regions
- 294 where subduction locking ends trenchward of a rigid backstop, interseismic subduction-related
- 295 shortening is localized in the region between the down-dip limit of locking and the rigid backstop
- 296 (McKenzie et al., 2022). The upper-plate region in southern Cascadia that is experiencing localized
- 297 subduction-related shortening due to this effect is also within the northern part of the MCC-corridor.
- 298 Further north, the weak-to-strong boundary is significantly closer to the trench (the Franciscan
- 299 complex is absent, and Siletz-Crescent terrane extends offshore) and locking extends beneath this
- weak-to-strong transition. McKenzie et al. (2022) find that in that case there is only a narrow region 300
- 301 of localized shortening offshore, west of the Siletz-Crescent terrane. Additionally the relatively
- 302 strong Siletz-Crescent terrane extends the subduction coupling signal far inland since it does not
- shorten easily. 303

283

- The subduction-related displacements observed by the geodetic stations are largely elastic and
- recovered during large megathrust events. However, typical of subduction zones globally, some
- fraction of this elastic deformation is retained as permanent upper-plate deformation over multiple
- 307 subduction earthquake cycles (e.g. McKenzie et al., 2022; Ramírez-Herrera et al., 2018; Saillard et
- al., 2017; Meltzner et al., 2006; Melnick et al., 2006). In contrast, the MCC-process produces
- permanent crustal shortening over millions of years, adjacent to and in advance of the MTJ. Although
- 310 the geodetic signal can be separated into subduction and NNW-components and records both elastic
- 311 (subduction) and permanent (subduction and MCC) deformation, the long-term deformation recorded
- 312 for example by slip on upper-plate faults and permanent uplift of the coastline records the
- 313 combined effects of permanent subduction and MCC deformation, which are not easily separated.

#### 3.3 Vertical Motions

314

- 315 Unlike the horizontal components of the GPS velocity field, the vertical component cannot be
- decomposed into separate signals related to different tectonic drivers based on direction. Instead the
- 317 geodetic uplift/subsidence signal records the combined vertical motions produced by all tectonic
- drivers in the region. Thus, although we observe present-day vertical motions of 1-4 mm/yr, by GPS
- and other geodetic indicators in the MCC corridor (Blewitt et al., 2018; Burgette et al., 2009) (Figure
- 320 7), we cannot separate this into a subduction-coupling and MCC signal without prior subduction
- 321 locking or MCC-model assumptions.
- 322 The subduction component of the vertical motion during the inter-earthquake interval largely
- depends on the location of the site relative to locking on the subduction plate interface and the time
- since the last megathrust earthquake. If the site lies above a locked region, we expect to record
- subsidence, however when the site is inboard of the locked region it could record subsidence, uplift
- or zero present-day vertical motion depending on the details of the coupling (Govers et al., 2018).
- 327 Some locking models for Cascadia (e.g. McKenzie et al., 2021; Li et al., 2018; Schmalzle et al.,
- 328 2014) find that locking extends near to and in some cases beneath the present-day coastline of
- 329 Cascadia. With that configuration we would generally expect subsidence along the coastline during
- the interseismic period. In southern Cascadia however, crustal thickening associated with the MCC-
- process produces some uplift in the vicinity of the MCC spatial footprint (Figure 4; Furlong &
- Govers, 1999). As a result, where the MCC process and subduction are both contributing to the
- vertical motions (within the MCC corridor), the observed total GPS velocity field records the
- summation of both processes. In cases where the subduction coupling signal is subsidence, the
- addition of MCC uplift may reduce that subsidence or even combine to produce uplift. In regions
- where the subduction coupling signal is uplift, the MCC contribution would increase the observed
- 337 uplift.

338

### 4 Seismic Tomography Crustal Structure

- The MCC model involves upper-plate crustal shortening and thickening in advance of the migrating
- MTJ, and subsequent crustal thinning after passage of the MTJ (Furlong and Govers, 1999). How
- that crustal thickening is converted into upper-plate deformation is less clear since the MCC model
- did not place constraints on potential out-of-plane deformation or specify deformation mechanisms
- for the shallow crust (Furlong & Govers, 1999). Additionally, the geologic structure of the region
- affected by MCC deformation is varied, that is the crust involved has changed substantially over the
- past 9-10 million years (Figures 3 & 4). Prior to ~ 10 Ma, the region of MCC shortening/thickening
- was bounded on the east by the SNGV block (Figure 2, 3, 4). However, by  $\sim 5$  Ma as the MTJ
- migrated northward, the upper-plate geologic framework in southern Cascadia underwent a transition

- from a Franciscan-Great Valley to a Franciscan-KMP configuration (Figures 3 & 4). This suggests
- 349 that prior to 5 Ma the SNGV block was playing a similar role in upper-plate deformation to the KMP
- 350 today. To understand how the MCC and SNGV affect upper-plate deformation, including permanent
- 351 uplift and the development of shear zones, we use the results from a recent seismic tomography study
- 352 (Figures 8 & 9; A. Villaseñor, K.P. Furlong, H. Benz, personal communication; Furlong et al., 2021),
- 353 to identify the 3D crustal nature of the processes that are driving upper-plate deformation
- 354 (specifically crustal thickening and thinning, permanent uplift, and faulting). Based on this present-
- 355 day 3D crustal structure and plate reconstructions of the region (Figures 2 & 4), we can explore how
- 356 the crustal structure and upper-plate deformation associated with each of these tectonic processes has
- evolved over time.
- 358 This seismic tomography imagery (Figures 8 & 9) shows systematic differences in the overall pattern
- of MCC crustal thickening behavior in the region bounded on the east by the SNGV block (south)
- versus the KMP (north). Horizontal depth slices and cross-sectional profiles highlight the primary
- 361 characteristics of the crustal structure in the region. There is a significant contrast in seismic velocity
- properties between the meta-sedimentary Franciscan complex and the adjacent SNGV block and
- 363 KMP. South of the MTJ, the Franciscan complex (p-wave velocities (Vp) of  $\sim$ 5.6-6.4 km s<sup>-1</sup>) and
- MCC crustal deformation (thickening/thinning) is bounded on the east by the SNGV block (Vp ~6.8-
- 8.0 km s<sup>-1</sup>), and on the west by the Pioneer Fragment ( $Vp \sim 6.8-8.0 \text{ km s}^{-1}$ ). North of the MTJ the
- Franciscan complex is bounded on the west by the Gorda slab (~6.8-8.0 km s<sup>-1</sup>). However, to the east
- we see that the Franciscan rocks impinge on and into the KMP crust ( $Vp \sim 6.4-6.8 \text{ km s}^{-1}$ ) (Figures 8
- 368 & 9).

385

- This implies that MCC driven upper-plate deformation was, and is still, localized within the
- Franciscan complex when adjacent to the SNGV block. In contrast, MCC-related deformation
- 371 appears to extend into the KMP crust, north of the SNGV block. In particular, a region of Franciscan
- 372 crust appears to have intruded > 30 km into the SW region of the KMP at  $\sim 10-30$  km depth (Figures
- 8 & 9). Associated with this, there is a ~10 km thick tubular body of what we interpret to be
- Franciscan material, that extends an additional ~80 km east into the KMP at ~20-30 km depth
- 375 (Figures 8 & 9). This injected/intruded crustal material (Vp 6.0-6.4 km s<sup>-1</sup>) has an oblate cylindrical
- shape and is surrounded by the higher velocity crustal material of the KMP. We take this to indicate a
- form of crustal flow as the Franciscan complex is over-thickened as part of the MCC process and is
- then able to wedge or inject itself into the adjacent KMP crust.
- 379 As well as this intrusion of the Franciscan material into the KMP crust primarily from the west-
- southwest, there is a separate region of high p-wave velocity ( $\sim$ 6.8-7.6 km s<sup>-1</sup>) material lying at  $\sim$ 15-
- 381 30 km depth beneath the south-eastern region of the KMP crust. This high velocity body can be seen
- to be a continuation of the Great Valley ultramafic body to the south and appears to extend ~50-100
- 383 km beneath the KMP to the north (Figures 8 & 9(b)). In contrast to the injected Franciscan crust, this
- material appears to lie below the KMP crust, underthrusting the SE margin of the KMP.

#### 4.1 Discussion of Seismic Tomography Results

- 386 The crustal-scale plate boundary structure plays an important role in the patterns of upper-plate
- deformation produced by the tectonic processes acting in southern Cascadia. In particular, crustal
- 388 kinematics and deformation driven by the MCC process and SNGV motion correlate well with many
- of the regions of ongoing deformation. We see evidence (e.g. thickened crust adjacent to the southern
- edge of the Gorda slab, that thins to the south) of the effects of MCC crustal deformation in the
- tomography imagery (Figures 8 & 9) associated with the transition from subduction to translation.

- There are several instances where the crustal structure observed in the tomography differs from that
- expected from the MCC model (Furlong & Govers, 1999). We interpret these to reflect differences in
- 394 the way that MCC crustal thickening is accommodated in the North American upper plate.
- The MCC-driven thickened crust in the region currently south of the present-day MTJ occurred when
- that location was the southernmost part of the Cascadia subduction plate boundary as the MTJ was
- approaching (Furlong and Govers, 1999). For example, at  $\sim$  9-10 Ma, when the MTJ was located
- 398 substantially further south (Figures 2 & 3), the locus of MCC shortening and crustal thickening (at
- and north of the MTJ) would have been bounded on the east side by an abrupt transition from the
- 400 Franciscan complex to the Great Valley crust. The region of MCC-related deformation is always
- bounded on the west by the subducting plate (north of the MTJ) and the Pioneer Fragment (Figures 2,
- 3, 8, 9) immediately south of the MTJ since both features migrate with the MTJ. The result of this
- 403 Franciscan-bounding crustal structure is that when the MTJ was south of approximately 39° N, the
- 404 corridor of MCC-deformation would have been restricted to a narrow channel of the Franciscan
- 405 complex between the Pioneer Fragment and the SNGV block. This is seen in the narrow width (< 100
- 406 km) of the thickened low seismic-velocity material in that region.
- 407 Over the past 3-5 million years, with the continued northward migration of the MTJ and SNGV
- block, the eastern margin of the MCC corridor changed from being defined by the SNGV block to
- 409 the KMP. Prior to the switch to the KMP, the MCC deformational channel widened as a result of the
- 410 northern segment of the Great Valley ultramafic block being oriented more northward (Figure 2).
- This switch from SNGV to the KMP acting as the eastern boundary to the deformational channel has
- also led to a substantial change in how MCC crustal thickening is accommodated. North of the MTJ.
- the MCC crustal thickening is still bounded on the west by the subducting slab but seems to intrude
- 414 into (or otherwise be emplaced within) the KMP crust. This low seismic-velocity Franciscan material
- appears to wedge the KMP crust apart, and flow and inject itself into the existing KMP crust (Figure
- 8 & 9); i.e. we see that the low-velocity material lies between two regions of KMP crust.
- Additionally, this low-velocity intrusion is not planar, as might be expected for a situation where the
- KMP over-thrusts the Franciscan crust. Instead, as seen in the tomographic cross-sections (Figure 9),
- 419 it is a cylindrical intrusion within the KMP crust. For these reasons and its continuity to the
- 420 Franciscan complex we interpret the low-velocity material to be injected Franciscan crust that has
- 421 undergone crustal flow in its emplacement.
- 422 Other possible explanations for this intra-crustal low-velocity material such as lithologic variations
- within the KMP, or thermal variations are harder to explain based on the geometry and extent of the
- region of anomalous crust. Additionally, starting at ~6 Ma, the SNGV block began to accelerate
- 425 (Plattner et al., 2010), converging with and pushing the KMP ahead of it. The tomography results
- 426 imply that as part of that convergence, Great Valley material that was initially in the gap between the
- SNGV and KMP prior to SNGV movement, appears to underthrust the southeastern margin of the
- 428 KMP. (Figures 8 & 9). During the Eocene to Miocene, exhumation (Piotraschke et al., 2015; Batt et
- al., 2010) of material in the footwall (north) of the La Grange fault lead to crustal thinning in the
- hanging wall to the south. This region of La Grange crustal thinning could have provided the space
- where we observe the northern limit of the emplaced Great Valley body beneath the KMP crust,
- potentially having replaced this previously exhumed material. This region of impingement or
- 433 underthrusting of the northern limits of the Great Valley body also serves as an eastern and southern
- bounding constraint on the region of the Franciscan crustal flow within the KMP, producing a nose-
- like protuberance of the lower-velocity material across the KMP.

- We interpret this major change in how MCC crustal deformation is accommodated, predominantly
- within the Franciscan complex and its interaction with the adjacent KMP, to generate different styles
- of upper-plate faulting and uplift throughout the region. In particular, patterns of upper-plate faulting
- and uplift in present-day southern Cascadia and the KMP are likely to be geologically recent (since ~
- 5 Ma) since most crustal shortening/thickening in the MCC model occurs at and just to the north of
- 441 the MTJ. In contrast, at latitudes south of  $\sim 39^{\circ}$ N (i.e. located in southern Cascadia at  $\sim 10-5$  Ma),
- MCC upper-plate deformation was restricted to a narrow zone < 100 km in width, bound by the rigid
- Great Valley block to the east. Since 5 Ma, this corridor of Franciscan material has been able to
- expand laterally (> 50 km) into the KMP. Thus, prior to  $\sim 5$  Ma we expect topographically a
- relatively narrow "ridge" (< 100 km wide) of uplift in the MCC corridor and from ~5 Ma to the
- present, we see that the MCC-shortening zone has widened across the boundary between the
- Franciscan and KMP crust. Therefore, the upper-plate deformational response to the MCC in present-
- day southern Cascadia, including the KMP, should be relatively recent (< 5 Ma), since it is only from
- 5 Ma that MCC deformation has been active in that region (Figures 3 & 4).
- The study area straddles the southern edge of the subducting Gorda slab and in addition to the effects
- 451 that this location has on processes such as the MCC, the behavior of the southern slab edge has also
- been proposed to affect asthenospheric mantle flow in the region (Zandt and Humphreys, 2008).
- Zandt and Humphreys (2008) proposed that if there is significant rollback of the Gorda slab that
- mantle flow could be induced around the southern edge of the slab, akin to the mantle flow inferred
- around the northern edge of the subducting Pacific slab at Tonga (e.g. Foley and Long, 2011). As
- discussed by Zandt and Humphreys (2008), such mantle flow is a longer wavelength feature that
- would be centered to the east, within (and underlying) the Basin and Range province. It also would
- likely be at greater depths than we are considering in this work, thus would have only a minor impact
- on our study region. Results of previous studies of mantle anisotropy along coastal North America
- indicate that our study region is within the mantle flow realm primarily affected by the local
- subduction and the lithospheric slab window. As shown by Hartog and Schwartz (2000) the upper-
- 462 most mantle anisotropy within the subduction domain is consistent with down-dip to the east flow,
- and in the slab window south of the southern edge of the Gorda slab, the mantle flow is similarly
- dipping down to the east likely indicating mantle upwelling into the slab window from the adjacent
- 465 mantle wedge, consistent with the geochemistry of the Coast Range volcanics erupted above the slab
- window (Furlong et al., 2003). The crustal flow of the Franciscan crust that we interpret to occur in
- 400 window (Furiong et al., 2003). The crustal flow of the Franciscan crust that we interpret to occur in
- the middle and lower crust, is separated from the upper-mantle flow regime by the lower crust and
- 468 lithospheric mantle of the North American plate.

469

### 4.2 Is the KMP undergoing active uplift?

- 470 The crustal structure, as seen in the tomography results, strongly correlates with the present day
- 471 topography in the Klamath and Siskiyou Mountains (Figure 9). We can see in the various
- 472 tomographic profiles a correlation between subsurface crustal structure (in particular, thickness of the
- Franciscan complex) and elevation. For example in profile A-A' (Figure 9(a)) the systematic
- 474 thickening of the Franciscan crust (from ~ 20 km to ~30-35 km) in association with MCC crustal
- deformation correlates with a nearly 2 km elevation change along the profile. The abrupt decrease in
- 476 crustal thickness and change in composition as the profile crosses from the Franciscan Coast Ranges
- 477 to the Great Valley is seen in a substantial drop in elevation.
- 478 Perhaps more diagnostic of the link between crustal structure and elevation are the correlations seen
- in profiles B-B' and C-C' (Figures 9(b), (c)). These profiles cut across the intruded nose of the
- Franciscan complex that we interpret to be intruded or injected into the KMP crust. The maximum
- elevation occurs at ~120-150 km along profile B-B', crossing this region. Profile C-C', which runs

- along the length of this Franciscan "nose" shows a systematic increase in elevation, that culminates
- in the region of Mt Eddy which sits above the eastern terminus of the low velocity body. Mt Eddy is
- 484 the highest elevation in the KMP, and is in a region of high local relief. We interpret that this reflects
- 485 the role that this crustal injection has played in driving uplift. The coincidence of the highest
- elevation above the eastern end of the material may indicate the time progression of uplift as the
- 487 crustal material flows eastward.
- Thermochronology studies from the KMP (apatite fission track (AFT) and apatite (U-Th)/He
- 489 (Piotraschke et al., 2015; Batt et al., 2010)) show that there have been two periods of regional cooling
- and exhumation within the province: (1) A late Cretaceous-Paleocene episode of regional cooling and
- exhumation; and (2) a Middle Tertiary (Eocene-Miocene, ~45-15 Ma) more localized episode of
- rapid exhumation of the footwall of the La Grange detachment fault (Cashman & Elder, 2002). This
- 493 faulting occurred with high slip rates of 2 mm/yr over ~30 million years (Piotraschke et al., 2015).
- The currently exposed surface is thought to have been brought to depths of ~2-3 km at the end of the
- latter unroofing event. If this exhumation event had continued to the present at moderate-high uplift
- rates, we would expect younger thermochronology ages as a consequence of deeper regions of the
- 497 crust being exhumed. The preservation of Eocene to early Miocene Apatite (U-Th)/He ages in
- samples implies minimal exhumation since the main unroofing event. As a result, evidence of current
- 499 exhumation likely reflects a relatively recent active process.
- Despite evidence for the most recent cooling/uplift being during the Eocene to Miocene, and minimal
- evidence of horizontal crustal shortening, the KMP is a topographically anomalous region of the
- southern Cascadia forearc, exhibiting higher elevations and topographic relief than the surrounding
- regions (Figures 1 & 10). One means of assessing whether differences in topography may be related
- to differential rock uplift involves looking at patterns of normalized channel steepness  $(k_{sn})$  across the
- region (e.g. Kirby & Whipple, 2012; Wobus et al., 2006; Kirby & Whipple, 2001; Whipple &
- Tucker, 1999). We use TopoToolbox 2 (Schwanghart & Scherler, 2014) to calculate the normalized
- channel steepness across the region using a reference concavity of 0.45 and create a smoothed  $k_{sn}$
- map shown in Figure 9. The drainage network  $k_{sn}$  map used in the interpolation is shown in Figure
- S2. When we compare these results to the seismic tomography imagery, we find there are spatial
- correlations between  $k_{sn}$  at the surface and inferred tectonic processes at depth.
- Our results show three key regions of elevated  $k_{sn}$ :
- 512 (1) There is a region of high  $k_{sn}$  in the northwestern-most KMP and the Siskiyou Mountains (Figure
- 513 10). This region is coincident with the highest present-day geodetic and benchmark (tide gauge and
- leveling) uplift rates observed along the Cascadia coastline (Figure 7, Blewitt et al. 2018, Burgette et
- al. 2009), and preliminary assessment of erosion and fluvial incision rates (Balco et al., 2013; Von
- Dassow & Kirby, 2017) suggest that this region is experiencing elevated erosion rates relative to the
- forearc to the north and west (Kirby et al., 2020).
- 518 (2) A large portion of the KMP itself has high values of  $k_{sn}$  compared to its surroundings, specifically
- between 41° N and 42.5° N. This area overlaps with the northern region of the low velocity
- intracrustal region imaged in the tomography, that we interpret to be an intrusion of Franciscan
- material into the KMP (Figure 10). This area is also in the footwall of the La Grange detachment
- fault, that underwent a period of exhumation during the Eocene to Miocene (Piotraschke et al., 2015;
- 523 Batt et al., 2010).

- 524 (3) South of the KMP there is a region of high  $k_{sn}$  in the Yolla Bolly mountains that coincides with
- 525 the thickest region of the MCC-thickened crust (Figures 8 & 10).
- 526 These observations suggest that there are three regions of the southern Cascadia forearc that may
- 527 currently be experiencing (or have very recently experienced) active tectonic uplift. In particular, the
- interior of the KMP may be undergoing a recent rejuvenation in uplift, perhaps associated with the
- onset of MCC- and SNGV-related deformation at ~6-5 Ma.

530

531

557

## 4.3 Possible Causes of Recent Uplift across Southern Cascadia

## 4.3.1 Uplift within the northwest KMP and Siskiyou Mountains

- The region of the northwestern-most KMP and the Siskiyou Mountains has both high  $k_{sn}$  and is
- experiencing some of the highest rates of present-day (2-4 mm/yr) uplift across the Cascadia margin
- 634 (Blewitt et al., 2018, Burgette et al., 2009, Figure 7). Uplifted marine terraces along the coast at these
- latitudes also indicate high long-term uplift rates ( $\sim 0.25 0.9$  mm/yr, Kelsey & Bockheim, 1994;
- Kelsey et al., 1994). Present-day horizontal GPS motions show significant NE- and NNW-directed
- shortening strain in the region (Figures 5 & 6). McKenzie & Furlong (2021) proposed that this
- NNW-directed shortening strain may be driven by the push of the SNGV block along the KMP's
- southern boundary. In addition to this NNW-directed tectonic driver, the results of McKenzie et al.
- 540 (2022) imply that this region of the Cascadia upper plate, between the down-dip limit of coupling and
- an upper-plate rigid backstop will be undergoing high rates of localized subduction-related
- shortening in response to coupling on the plate interface. The combination of subduction-related
- shortening strain and NNW-directed shortening strain could explain the high present-day geodetic
- 544 uplift and high topographic relief in this region.

### 545 4.3.2 Rejuvenation of Uplift of the KMP

- The subduction and NNW-directed components of the GPS velocity field show that at present the
- 547 KMP is accommodating low rates of NE- and NNW-oriented shortening ( $\sim 10^{-16} \text{ s}^{-1}$ ) (Figures 5 & 6).
- Thus, bulk crustal thickening of the KMP is an unlikely mechanism for driving recent uplift. We
- have interpreted the intracrustal low velocity body in the seismic tomography slices (Figures 8 & 9)
- to be Franciscan crustal material that has thickened and intruded into the KMP at mid-crustal levels
- as a consequence of crustal flow. We hypothesize that localized NNW-directed shortening,
- superimposed on NE-directed subduction-driven deformation, enables Franciscan crust to intrude
- into the KMP along a plane of weakness at depth. This injection of additional crustal material at
- depth into the KMP, would drive differential rock uplift within the KMP, providing an explanation
- for relatively recent uplift and generation of topographic relief. These effects associated with the
- MCC have only been affecting upper-plate deformation in this region since ~5 Ma (Figure 4).

### 4.3.3 Uplift within the southern MCC corridor

- South of the KMP, the region of high  $k_{sn}$  correlates with the thickest (>30 km thick) crust within the
- MCC corridor (Figures 8, 9, 10). South of this region the extensional (later stage) effects of the MCC
- are expected, and we see a systematically thinning crust, and active volcanism within the Clear Lake
- Volcanic field (Furlong & Schwartz, 2004; Furlong & Govers, 1999). This region of the upper plate
- is where the MCC model shows a transition from shortening strain (to the north) to extensional strain
- 563 (to the south), and thus we might expect that this region in response to MCC effects should not be
- experiencing significant active uplift at present (Furlong & Govers, 1999). However, a few million
- years ago this region would have been shortening and thickening, similar to the upper plate currently

566 in the vicinity of the MTJ. Thus, this region of high  $k_{sn}$  may be recording the channel response to a transition from an actively shortening to an actively thinning crust. 567

#### 5 **Faulting and Shear Zone Development**

568

- 569 In addition to numerous accretionary margin faults linked to displacements on the megathrust 570 detachment offshore near to the trench, there are several active crustal-scale upper-plate structures 571 onshore within the Franciscan and KMP crust. In southern Cascadia, these faults are being loaded by 572 the composite set of forces associated with both subduction and NNW-directed shortening and shear 573 (McKenzie & Furlong, 2021; McCrory, 2000; Kelsey & Carver, 1988). Additionally, with the 574 generally NNW/NW strike of these faults (e.g. the Grogan fault, Figure 11), they are optimally 575 oriented for both reverse dip-slip in response to subduction-related SW-NE shortening and right-576 lateral shear motion west of the KMP (Figures 5 & 11). As the MTJ migrates northward, these faults 577 are well oriented to participate in the developing San Andreas plate boundary. These faults 578 potentially undergo a change in their behavior over time from dominantly dip-slip to dominantly 579 strike-slip motion as the MTJ approaches and the plate boundary transitions from subduction to 580 transform. Initially, such faults would likely exhibit reverse motions, due to subduction coupling 581 related NE-directed shortening of the upper plate. As the MTJ moves further north, a right-lateral 582 shear zone develops along the western margin (Figures 5 & 11). As a consequence, NNW-oriented 583 faults within the right-lateral shear zone, such as the Grogan fault, the Lost Man fault and faults 584 within the Bald Mountain fault zone (Figure 11) are loaded by both right-lateral shear strain and 585 subduction-related shortening strain. During this time interval, these faults could experience reverse, 586 oblique or right-lateral motion. As the MTJ continues its northward advance and this upper-plate 587 crust transfers from the Cascadia subduction zone to the San Andreas (Pacific-North America) plate 588 boundary, the NNW-oriented faults become loaded by right-lateral shear stresses, developing further 589 as San Andreas plate boundary structures.
- 590 It is unclear when these subduction zone upper-plate faults are primarily active – whether coincident 591 with megathrust rupture or during times between major subduction zone events. There is a set of 592 faults that occupy a similar location within the transition zone at the southern end of the Hikurangi 593 subduction zone (in northern South Island, New Zealand) to strike-slip motion along the Alpine fault 594 system (Furlong and Herman, 2017). These upper-plate faults experienced extreme vertical and 595 strike-slip motion during the 2016 Kaikoura megathrust earthquake (Hamling et al., 2017), which 596 involved simultaneous rupture of the megathrust and these upper-plate faults. If the equivalent upper-597 plate faults in southern Cascadia behave similarly, this could explain the large, permanent vertical 598 motion observed along the southern Cascadia coastline, documented by uplifted marine terrace 599 platforms (Padgett et al. 2019; Kelsey et al., 1994; Kelsey & Bockheim, 1994; Muhs et al., 1992; 600 Kelsey, 1990).

#### 6 **Conclusions**

601

602 The overall deformational effects on the upper plate of the southern Cascadia forearc from the 603 superposition of multiple tectonic processes, including subduction coupling, the MCC process, and the northward motion of the SNGV block can be identified by consideration of the decadal-scale 604 605 motions of the upper plate and the regional long-term geomorphic and geologic record. In regions 606 where subduction coupling is not the sole contributor to upper-plate deformation, for example near 607 plate boundary transition zones such as the MTJ region, understanding the upper-plate effects of 608

superposed tectonic processes is important. Being able to separate these effects is crucial when using

- of upper-plate observations to determine the characteristics of subduction zone processes such as plate
- 610 interface coupling.
- In addition to the primary role of subduction coupling, upper-plate deformation in Cascadia is also
- affected by shortening driven by the migration of the MTJ and SNGV block, acting on varying
- on the location of upper-plate terrane boundaries. From the mid-
- Miocene to the present, the nature of the interactions between these geological terranes with the
- 615 tectonic drivers has changed significantly as a consequence of the migration of the MTJ. At ~15 Ma,
- the KMP was in central Cascadia and subduction coupling was the main tectonic driver in that
- region. At that time the primary role of the SNGV block was as the rigid backstop inboard of the
- Franciscan complex. As the MTJ migrated northward, the KMP became the backstop east of the
- Franciscan complex, and the SNGV became a driver of NNW-directed deformation in southern
- 620 Cascadia.
- The crustal architecture both within the primary MCC deformational corridor, and its bounding
- terranes, has a significant impact on how the crustal thickening and thinning occurs. South of the
- MTJ, the MCC-related deformation of the Franciscan complex was constrained to a relatively narrow
- region between the Pioneer fragment and the SNGV block, when the MTJ was further south. In this
- case the effects of the MCC on uplift would have been restricted to this narrow channel (Figure 11).
- In contrast, deformation of the Franciscan complex north of the MTJ, where the bounding terrane to
- the east is the KMP, is not constrained to a narrow channel. Instead, from seismic tomography
- imagery we see that in addition to crustal shortening and thickening within the MCC corridor, the
- 629 thickened Franciscan complex is able to flow and intrude into the KMP at mid-crustal levels (Figures
- 8, 9 & 11). This intruded Franciscan crust primarily deforms the western margin of the KMP, but
- there is also a narrow injection of this material further eastward into the KMP (Figures 8 & 9). The
- MCC has only been contributing to upper-plate deformation in this region since ~5 Ma, and as a
- result this intracrustal flow and injection is most likely a relatively young feature, that will continue
- 634 to propagate northward with the MTJ. Similarly, the underthrusting of the Great Valley ultramafic
- body beneath the SE margin of the KMP, which we interpret from the seismic tomography, could
- continue to propagate northward with the SNGV block. We find that the impingement of the
- 637 Franciscan material and the Great Valley ultramafic body on the KMP may be generating a
- rejuvenation of uplift of the KMP since ~5 Ma, inferred from high channel steepness within the
- interior of the KMP at present.

## **7** Figure Captions

- Figure 1. Tectonic and geological setting of the study region and surrounding area. (a) Topographic
- map of the northwest North America (SW British Columbia, Washington, Oregon, northern
- 643 California, and NW Nevada). The names of key geographic and geologic features and provinces are
- labeled (in yellow on land and in white offshore). BFZ = Blanco Fracture Zone, MFZ = Mendocino
- Fracture Zone, MTJ = Mendocino Triple Junction, WGB = Western Great Basin, KMP = Klamath
- Mountain province, LGD = La Grange detachment, LMF = Lost Man fault, BMFZ = Bald Mountain
- oro Mountain province, Edd La Grange detachment, Ewit Lost Main raun, Bivit Z Daid Mountain
- fault zone, GF = Grogan fault, ERFZ = Eaton Roughs fault zone, LMFZ = Lake Mountain fault zone.
- 648 (b) Kinematic setting of the study region showing present-day motions of the Juan de Fuca plate,
- Pacific plate and SNGV crustal block with respect to North America (DeMets et al., 2010; d'Alessio
- et al., 2005). The blue shaded region is the extent of the subducting slab at depth from Slab2 (Hayes,
- 2018), and the dark blue lines are the 10 km slab contours. The KMP, the SNGV block, and the
- 652 ECSZ are outlined and shaded in orange, green and red respectively. (c) Geological map of the study
- 653 region.

640

- 654 Figure 2. Schematic plate reconstruction of the study region at ~15 Ma (a) and the present day (b).
- The locations of key geological and tectonic terranes are highlighted. The study area is outlined by a
- dashed black box. At ~15 Ma (a) the study area (present-day southern Cascadia) is in central
- 657 Cascadia. At present (b) the study area is within southern Cascadia. Reconstructions were done using
- 658 the SNGV-North America Euler stage pole (d'Alessio et al., 2005), Pacific Juan de Fuca Euler
- poles (Wilson, 1993) and Pacific-North America Euler poles (DeMets & Merkouriev, 2016).
- Figure 3. Schematic plate reconstruction of the region from  $\sim$ 35 Ma 5 Ma. The locations of key
- geological and tectonic terranes are highlighted. (a) ~35 Ma, (b) ~30 Ma, (c) ~25-20 Ma, (d) ~10-5
- 662 Ma.
- Figure 4. Plate reconstructions showing the total (subduction plus NNW-directed processes) synthetic
- 664 GPS velocities for the region from 9 Ma to present-day. The KMP is outlined and shaded in orange,
- the Sierra Nevada/Great Valley (SNGV) block is outlined and shaded in green, and the approximate
- spatial extend of deformation (thickening and thinning) associated with the MCC is outlined and
- shaded in blue. (a) ~9 Ma, (b) ~5 Ma, (c) present-day. Reconstructions were done using the SNGV-
- North America Euler stage pole (d'Alessio et al., 2005), Pacific Juan de Fuca Euler poles (Wilson,
- 1993) and Pacific-North America euler poles (DeMets & Merkouriev, 2016).
- Figure 5. Transects through the present-day NNW-directed and subduction-related GPS decomposed
- velocity fields. (a) NNW transect (south to north) through the NNW-directed velocity field within the
- MCC corridor the Franciscan complex west of the KMP. Red vectors within the map (top) are the
- velocities (both grey and red circles) shown in the profile (bottom). The grey circles are vectors over
- 674 25 km from the profile line. (b) NNW transect (south to north) through the NNW-directed velocity
- 675 field within the KMP. Red vectors within the map (top) are the velocities (red circles) shown in the
- profile (bottom). (c) NE transect (west to east) through the NNW-directed velocity field through the
- MCC corridor and the KMP. Pink vectors within the map (top) are the velocities (pink circles) shown
- in the profile (bottom).
- Figure 6. (a) NE-directed (subduction coupling) component of the GPS velocity field in the study
- region. Data (blue vectors) sampled by the NE transects (west to east) shown are plotted in (b). (b)
- Profile through the NE-directed GPS velocity field (profiles shown in (a)). The blue transparent line
- is the synthetic GPS velocity model result for a finite element model with an upper plate composed
- of weak material (the Franciscan complex and modern accretionary margin) near to the trench, and a
- rigid backstop (the KMP) inboard. The weak to strong boundary in the model is at 160 km (the
- approximate distance of the KMP boundary from the trench). (c) Shortening strain rate derived from
- model velocity results in (b). The uplift rate is based on the assumption of an average upper-plate
- thickness of 20 km (adapted from McKenzie et al., 2022).
- Figure 7. Present-day uplift rates across the southern Cascadia forearc. (a) Graph of uplift versus
- latitude for GPS (black squares) and benchmark leveling data (white circles) from coastal regions in
- 690 southern Cascadia (125 °W 123 °W) (Blewitt et al., 2018; Burgette et al., 2009). (b) Map of
- present-day uplift rates. The circles are benchmark level data (Burgette et al., 2009) and the squares
- are GPS vertical motions (Blewitt et al., 2018). The semi-transparent interpolated uplift shown in the
- background is derived from a grid of the GPS vertical motions with a grid size of 10 km, and
- masking threshold of 30 km. The dashed red line is the approximate eastern extent of the maximum
- 695 upper-plate uplift signal in the region.

- Figure 8. Seismic tomography results in map view at different crustal levels (10 km, 20 km and 25
- 697 km) (Furlong et al., 2021). The Great Valley body, the Pioneer fragment, the Gorda slab, the
- 698 Franciscan complex and the Sierra Nevada are labeled. Pink dashed lines are 10 km slab contours
- 699 (Slab2, Hayes 2018). Lines A-A', B-B', C-C' and D-D' indicate the locations for the cross sectional
- profiles shown in Figure 9.
- Figure 9. Seismic tomography cross sections A-A', B-B', C-C' and D-D'. Topographic swath profiles
- for each cross-section are shown above. The swaths used in the topographic profiles are shown in
- Figure S3. Cross section lines are shown in Figures 8 and 10. The green dashed line shows the
- approximate extent of the Gorda slab and Pioneer fragment beneath North America. The approximate
- locations of the surface boundaries for the geologic terranes are labeled at the top of each cross
- section.
- Figure 10. Interpolated channel steepness  $(k_{sn})$  for the region of southern Cascadia. The blue dashed
- line shows the extent of the Pioneer fragment from the tomography results. The black dashed lines
- shows the approximate extend of low velocity (Franciscan) material within the KMP, derived from
- 710 the tomography results. The white and yellow solid lines are the 6.4 km/s p-wave velocity contours
- from the tomography imagery at 20 km and 25 km depth respectively, that we interpret represent the
- extent of the thickened Franciscan crust at those depths. The purple dashed line is the 25 km depth of
- the 6.8 km/s p-wave velocity contour, that we interpret to outline the Great Valley ultramafic body at
- 714 that depth.
- Figure 11. Summary map showing the tectonic setting, geographic regions, and key tectonic
- processes acting in the study region that produce upper-plate deformation of the North America plate.
- North of ~43 °N subduction-coupling in the dominant tectonic process acting to deform the upper
- 718 plate. The light grey shaded region shows the approximate N-S extent of the MCC process on the
- 719 upper plate. The dark grey shading shows the region of the highest crustal thickness within the MCC
- 720 corridor, outlined based on the 20 km depth tomography imagery. The horizontal dashed region
- within the KMP, shows the approximate extend of the Franciscan crustal material injected into the
- KMP at mid-crustal levels. The Pioneer fragment is shaded in light blue. The teal shaded region is
- the SNGV block. The dotted lined region within the SNGV block shows the approximate extent of
- the Great Valley ultramafic body at mid-crustal levels.

### 725 **8** Conflict of Interest

- 726 The authors declare that the research was conducted in the absence of any commercial or financial
- 727 relationships that could be construed as a potential conflict of interest.

### 728 **9 Author Contributions**

- KAM analysed the GPS and topographic data. KAM, KPF and EK interpreted the results. KAM was
- 730 the main contributor in writing the manuscript and KAM, KPF and EK were involved in writing and
- editing the final manuscript. All authors read and approved the final manuscript.

## **732 10 Funding**

733 This work was supported by the National Science Foundation under the Award EAR175781.

### 734 11 Acknowledgments

- We thank the National Science Foundation who provided support for this research. We thank the two
- reviewers for their comments that helped improve the manuscript.
- 737 12 References
- Angster, S., Wesnousky, S., Figueiredo, P., Owen, L.A., & Sawyer, T. (2020). Characterizing strain
- between rigid crustal blocks in the southern Cascadia forearc: Quaternary faults and folds of the
- northern Sacramento Valley, California. Geology, 49(4), 287-291. doi:
- 741 <u>https://doi.org/10.1130/G48114.1</u>
- Argus, D.F. & Gordon, R.G. (1991). Current Sierra Nevada-North America motion from very long
- baseline interferometry: Implications for the kinematics of the western United States, Geology, 19.
- 744 1085-1088. doi: https://doi.org/10.1130/0091-7613(1991)019<1085:CSNNAM>2.3.CO;2
- Atwater, T. (1970). Implications of Plate Tectonics for the Cenozoic Tectonic Evolution of Western
- North America. GSA Bulletin, 81(12), 3513-3536. doi: https://doi.org/10.1130/0016-
- 747 <u>7606(1970)81[3513:IOPTFT]2.0.CO;2</u>
- Balco, G., Finnegan, N., Gendaszek, A., Stone, J.O.H., Thompson, N. (2013). Erosional response to
- northward-propagating crustal thickening in the coast ranges of the U.S. Pacific Northwest.
- 750 American Journal of Science, 313(8), 790-806. doi: https://doi.org/10.2475/11.2013.01
- 751 Batt, G.E., Cashman, S.M., Garver, J.I., & Bigelow, J.J. (2010). Thermotectonic Evidence for Two-
- 752 Stage Extension on the Trinity Detachment Surface, Eastern Klamath Mountains, California.
- 753 American Journal of Science, 310, 261-281. doi: https://doi.org/10.2475/04.2010.02
- Beaudoin, B.C., Godfrey, N.J., Klemperer, S.L., Lendl, C., Tréhu, A.M., Henstock, T.J., Levander,
- A., Holl, J.E., Meltzer, A.S., Luetgert, J.H., & Mooney, W.D. (1996). Transition from slab to
- slabless: Results from the 1993 Mendocino triple junction seismic experiment. Geology, 24(3), 195-
- 757 199. doi: https://doi.org/10.1130/0091-7613(1996)024<0195:TFSTSR>2.3.CO;2
- 758 Beaudoin, B.C., Hole, J.A., Klemperer, S.L., & Tréhu, A.M. (1998). Location of the southern edge of
- 759 the Gorda slab and evidence for an adjacent asthenospheric window: Results from seismic profiling
- and gravity. JGR: Solid Earth, 103(B12), 30101-30115. doi: https://doi.org/10.1029/98JB02231
- 761 Bennett, G.L., Miller, S.R., Roering, J.J., & Schmidt, D.A. (2016). Landslides, threshold slopes, and
- the survival of relict terrain in the wake of the Mendocino Triple Junction. Geology, 44(5), 363-355.
- 763 doi: https://doi.org/10.1130/G37530.1
- Bennett, R.A., Davis, J.L., & Wernicke, B.P. (1999). Present-day pattern of Cordilleran deformation
- 765 in the western United States. Geology, 27(4), 371-374. doi: https://doi.org/10.1130/0091-
- 766 7613(1999)027<0371:PDPOCD>2.3.CO;2
- Bennett, R.A., Wernicke, B.P., Niemi, N.A., Friedrich, A.M., & Davis J.L. (2003). Contemporary
- strain rates in the northern Basin and Range province from GPS data. Tectonics, 22(2). doi:
- 769 https://doi.org/10.1029/2001TC001355
- 770 Blewitt, G., Hammond, W.C., & Kreemer, C. (2018). Harnessing the GPS Data Explosion for
- 771 Interdisciplinary Science. Eos, 99. doi: https://doi.org/10.1029/2018EO104623

- Burgette R.J., Weldon R.J. II, & Schmidt D.A. (2009). Interseismic uplift rates for western Oregon
- and along-strike variation in locking on the Cascadia subduction zone. JGR: Solid Earth. doi:
- 774 https://doi.org/10.1029/2008JB005679
- Cashman, S.M., & Elder, D.R. (2002). Post-Nevadan detachment faulting in the Klamath Mountains,
- 776 California. GSA Bulletin, 114(12), 1520-1534. doi: <a href="https://doi.org/10.1130/0016-">https://doi.org/10.1130/0016-</a>
- 777 7606(2002)114<1520:PNDFIT>2.0.CO;2
- D'Alessio, M.A., Johanson, I.A., Bürgmann, R., Schmidt, D.A., & Murray, M.H. (2005). Slicing up
- the San Francisco Bay Area: Block kinematics and fault slip rates from GPS-derived surface
- velocities. JGR Solid Earth, 110(B6). doi: https://doi.org/10.1029/2004JB003496
- DeMets C., Gordon R.G., & Argus D.F. (2010). Geologically current plate motions. Geophys J Int,
- 782 181(1), 1–80. doi: https://doi.org/10.1111/j.1365-246X.2009.04491.x
- 783 DeMets, C., & Merkouriev, S. (2016). High-resolution reconstructions of Pacific-North America
- plate motion: 20 Ma to present. Geophysical Journal International, 207(2), 741-773. doi:
- 785 <u>https://doi.org/10.1093/gji/ggw305</u>
- Dickinson, W.R., & Snyder, W.S. (1979). Geometry of triple Junctions related to San Andreas
- 787 Transform. JGR: Solid Earth, 84(B2), 561-572. doi: <a href="https://doi.org/10.1029/JB084iB02p00561">https://doi.org/10.1029/JB084iB02p00561</a>
- Dixon, T.H., Miller, M., Farina, F., Wang, H., & Johnson, D. (2000). Present-day motion of the
- 789 Sierra Nevada block and some tectonic implications for the Basin and Range province, North
- 790 America Cordillera. Tectonics, 19(1), 1-24. doi: <a href="https://doi.org/10.1029/1998TC001088">https://doi.org/10.1029/1998TC001088</a>
- 791 Ernst, W.G. (2013). Earliest Cretaceous Pacificward offset of the Klamath Mountains salient, NW
- 792 California-SW Oregon. Lithosphere, 5(1), 151-159. doi: https://doi.org/10.1130/L247.1
- Furlong, K.P. (1984). Lithospheric behavior with triple junction migration: an example based on the
- Mendocino triple junction. Physics of the Earth and Planetary Interiors, 36(3-4), 213-223. doi:
- 795 https://doi.org/10.1016/0031-9201(84)90047-5
- Furlong, K.P., & Govers, R. (1999). Ephemeral crustal thickening at a triple junction: The
- Mendocino crustal conveyor. Geology, 27(2),127-130. doi: https://doi.org/10.1130/0091-
- 798 <u>7613(1999)027<0127:ECTAAT>2.3.CO;2</u>
- Furlong, K.P., & Herman, M.W. (2017). Reconciling the deformational dichotomy of the 2016 Mw
- 7.8 Kaikoura New Zealand earthquake. Geophysical Research Letters, 44(13), 6788-6791. doi:
- 801 https://doi.org/10.1002/2017GL074365
- Furlong, K.P., Lock, J., Guzofski, C., Whitlock, J., & Benz, H. (2003). The Mendocino Crustal
- 803 Conveyor: Making and Breaking the California Crust. International Geology Review, 45(9). doi:
- 804 https://doi.org/10.2747/0020-6814.45.9.767
- Furlong, K., McKenzie, K.A., Villaseñor, A., Benz, H. (2021). Linkage Between Upper-Plate
- 806 Cascadia Faulting and the Evolution of the Northern San Andreas Plate Boundary Fault System.
- 687 GSA Connects 2021, Portland, Oregon: Paper No. 36-2. Geological Society of America Abstracts
- with Programs, v. 53, no. 6. doi: https://doi.org/10.1130/abs/2021AM-367654

- Furlong, K.P., & Schwartz, S.Y. (2004). Influence of the Mendocino Triple Junction on the Tectonics
- of Coastal California. Annual Review of Earth and Planetary Sciences, 32, 403-433. doi:
- 811 https://doi.org/10.1146/annurev.earth.32.101802.120252
- Foley, B.J., Long, M.D. (2011). Upper ad mid-mantle anisotropy beneath the Tonga slab.
- 813 Geophysical Research Letters, 38(L02303). doi: https://doi.org/10.1029/2010GL046021
- Godfrey N.J., Beaudoin, B.C., Klemperer, S.L., Mendocino Working Group (1997). Ophiolitic
- 815 <u>basement to the Great Valley forearc basin, California, from seismic and gravity data: Implications</u>
- for crustal growth at the North American continental margin. GSA Bulletin, 109(12), 1536-1563. doi:
- 817 https://doi.org/10.1130/0016-7606(1997)109<1536:OBTTGV>2.3.CO;2
- Govers R., Furlong, K.P., van de Wiel, L., Herman, M.W., & Broerse, T. (2018). The Geodetic
- 819 Signature of the Earthquake Cycle at Subduction Zones: Model Constraints on the Deep Processes.
- 820 Reviews of Geophysics, 56(1), 6-49. doi: https://doi.org/10.1002/2017RG000586
- 621 Guzofski, C., & Furlong, K.P. (2002). Migration of the Mendocino triple junction and ephemeral
- 822 crustal deformation: Implications for California Coast Range heat flow. Geophysical Research
- 823 Letters, 29(1), 12-1 12-4. doi: https://doi.org/10.1029/2001GL013614
- Hamling, I.J., Hreinsdóttir, S., Clark, K., Elliott, J., Liang C., Fielding, E., Litchfield, N., Villamor,
- P., Wallace, L., Wright, T.J., D'Anastasio E., Bannister, S., Burbidge, D., Denys, P., Gentle, P.,
- Howarth, J., Mueller, C., Palmer, N., Pearson, C., Power, W., Barnes, P., Barrell, D.J.A., Van Dissen,
- 827 R., Langridge, R., Little, T., Nicol, A., Pettinga, J., Rowland, J., & Stirling, M. (2017). Complex
- multifault rupture during the 2016 Mw 7.8 Kaikōura earthquake, New Zealand, Science, 356(6334).
- 829 doi: https://doi.org/10.1126/science.aam7194
- Hartog, R., Schwartz, S.Y. (2000). Subduction-induced strain in the upper mantle east of the
- Mendocino Triple Junction, California. JGR: Solid Earth, 105(B4), 7909-7930. doi:
- 832 https://doi.org/10.1029/1999JB900422

833

- Hayes, G. (2018). Slab2 A Comprehensive Subduction Zone Geometry Model. U.S. Geological
- 835 Survey data release. doi: https://doi.org/10.5066/F7PV6JNV

836

- 837 Irwin, W.P. (1985). Age and Tectonics of Plutonic Belts in Accreted Terranes of the Klamath
- 838 Mountains, California and Oregon. In Tectonostratigraphic terranes of the circum-Pacific
- 839 region: Circum-Pacific Council for Energy and Mineral Resources, Earth Science Series
- 840 Number 1, Howell D.G. (ed.), 187-199

841

- Kelsey, H.M. (1990). Late Quaternary Deformation of Marine Terraces on the Cascadia Subduction
- Zone near Cape Blanco, Oregon. Tectonics, 9(5), 983-1014. doi:
- 844 https://doi.org/10.1029/TC009i005p00983

845

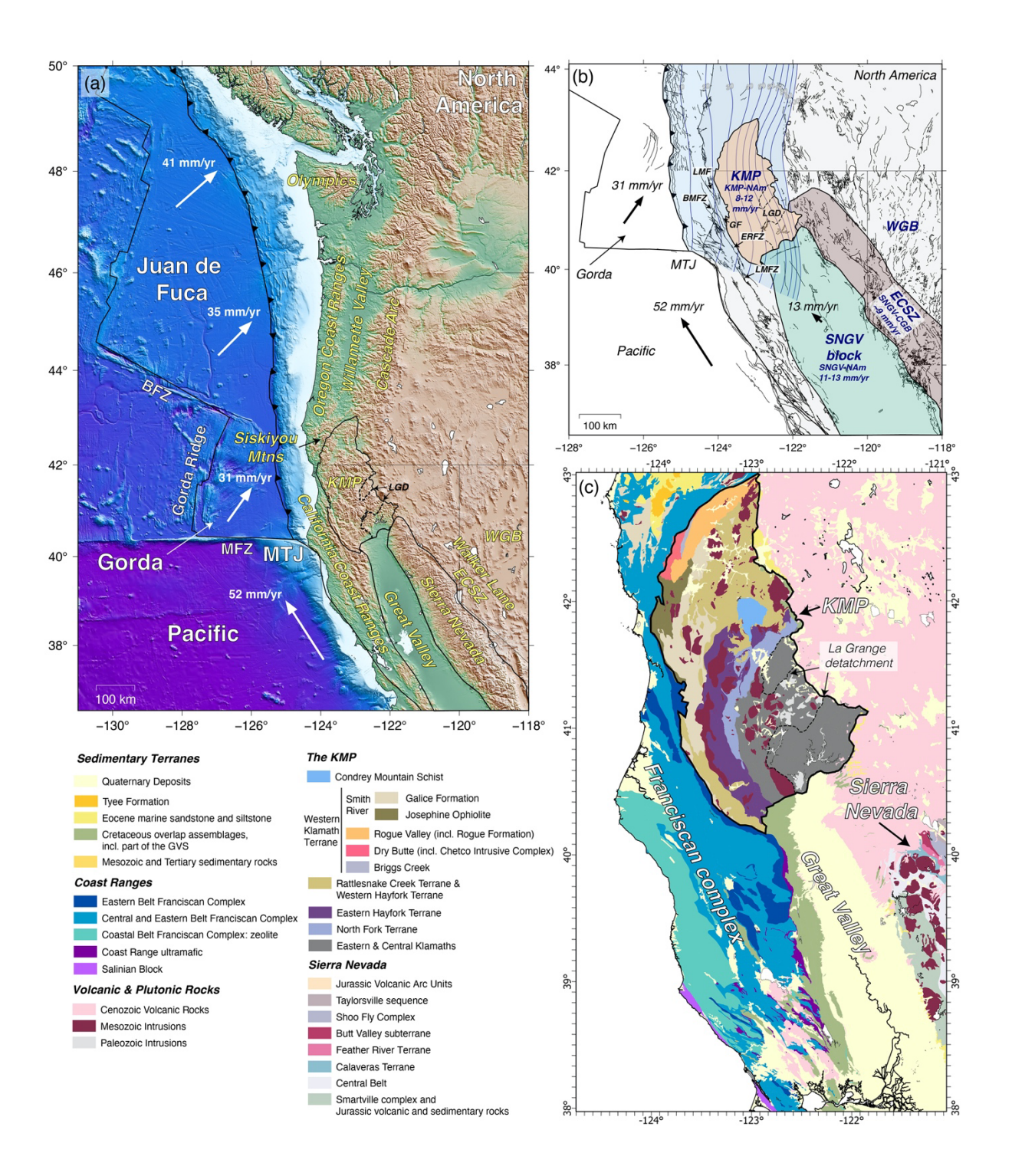
- Kelsey, H.M., & Bockheim, J.G. (1994). Coastal landscape evolution as a function of eustasy and
- 847 surface uplift rate, Cascadia margin, southern Oregon. GSA Bulletin, 106, 840-854. doi:
- 848 https://doi.org/10.1130/0016-7606(1994)106<0840:CLEAAF>2.3.CO;2
- Kelsey, H.M., & Carver, G.A. (1988). Late Neogene and Quaternary tectonics associated with
- 850 northward growth of the San Andreas Transform Fault, northern California. JGR: Solid Earth
- 93(B5):4797-4819. doi: https://doi.org/10.1029/JB093iB05p04797

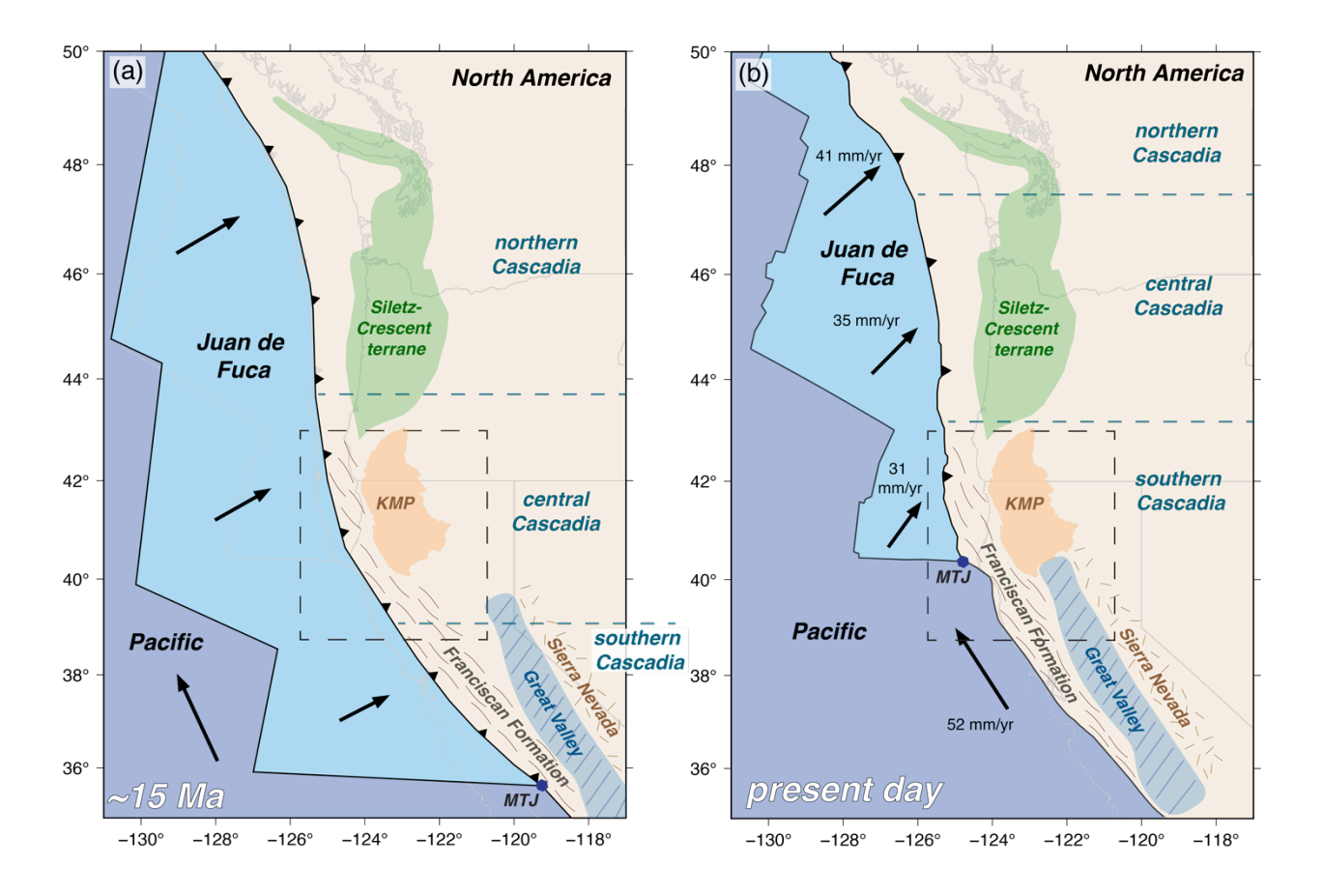
- Kelsey, H.M., Engebretson, D.C., Mitchell, C.E., & Ticknor, R.L. (1994). Topographic form of the
- 853 Coast Ranges of the Cascadia Margin in relation to coastal uplift rates and plate subduction. JGR:
- 854 Solid Earth, 99(B6), 12245-12255. doi: https://doi.org/10.1029/93JB03236
- Kirby, E., McKenzie, K.A., Furlong, K., & Hefner, W. (2021). Geomorphic Fingerprint of Active
- Faults in the Southern Cascadia Forearc and their Geodynamic Significance. GSA Connects 2021,
- Portland, Oregon: Paper No. 30-3. Geological Society of America Abstracts with Programs, v. 53,
- 858 no. 6. doi: https://doi.org/10.1130/abs/2021AM-370126
- Kirby, E., Furlong, K.P., von Dassow, W., Worms, K., McKenzie, K., & Mahan, S.A. (2020). Does
- 860 Topography Along the Cascadia Forearc Reflect Permanent Deformation of North America? GSA
- 861 Connects 2020: Paper No. 240-3. Geological Society of America Abstracts with Programs, v. 52, no.
- 862 6. doi: <a href="https://doi.org/10.1130/abs/2020AM-357618">https://doi.org/10.1130/abs/2020AM-357618</a>
- Kirby, E., & Whipple, K.X. (2001). Quantifying differential rock-uplift rates via stream profile
- analysis. Geology, 29(5), 415-418. doi: <a href="https://doi.org/10.1130/0091-">https://doi.org/10.1130/0091-</a>
- 865 7613(2001)029<0415:QDRURV>2.0.CO;2
- Kirby, E., & Whipple, K.X. (2012). Expression of active tectonics in erosional landscapes. Journal of
- 867 Structural Geology, 44, 54-75. doi: <a href="https://doi.org/10.1016/j.jsg.2012.07.009">https://doi.org/10.1016/j.jsg.2012.07.009</a>
- Li, S., Wang, K., Wang, Y., Jiang, Y., & Dosso, S.E. (2018). Geodetically Inferred Locking State of
- the Cascadia Megathrust Based on a Viscoelastic Earth Model. JGR: Solid Earth, 123(9), 8056-8072.
- 870 doi: https://doi.org/10.1029/2018JB015620
- Lock J, Kelsey H, Furlong K, Woolace A (2006). Late Neogene and Quaternary landscape evolution
- of the northern California Coast Ranges: Evidence for Mendocino triple junction tectonics. GSA
- 873 Bulletin, 118(9/10):1232-1246. doi: https://doi.org/10.1130/B25885.1
- McCaffrey R., King R.W., Payne S.J., & Lancaster M. (2013). Active tectonics of northwestern U.S.
- inferred from GPS-derived surface velocities. JGR Solid Earth 118(2):709-723. doi:
- 876 https://doi.org/10.1029/2012JB009473
- McCaffrey, R., Long, M.D., Goldfinger, C., Zwick, P.C., Nabelek, J.L., Johnson, C.K., & Smith, C.
- 878 (2000). Rotation and plate locking at the Southern Cascadia Subduction Zone. Geophysical Research
- 879 Letters, 27(19), 3117-3120. doi: https://doi.org/10.1029/2000GL011768
- McCaffrey R., Qamar A.I., King R.W., Wells R., Khazaradze G., Williams C.A., Stevens C.W.,
- Vollick J.J., Zwick P.C. (2007). Fault locking, block rotation and crustal deformation in the Pacific
- Northwest. Geophysical Journal International 169(3):1315-1340. doi: https://doi.org/10.1111/j.1365-
- 883 246X.2007.03371.x
- McCrory, P.A. (2000). Upper plate contraction north of the migrating Mendocino triple junction,
- northern California: Implications for partitioning of strain. Tectonics, 19(6):1144-1160. doi:
- 886 https://doi.org/10.1029/1999TC001177
- McCrory, P.A., & Wilson, D.S. (2013). A kinematic model for the formation of the Siletz-Crescent
- forearc terrane by capture of coherent fragments of the Farallon and Resurrection plates, Tectonics,
- 889 32(3), 718-736. doi: <a href="https://doi.org/10.1002/tect.20045">https://doi.org/10.1002/tect.20045</a>

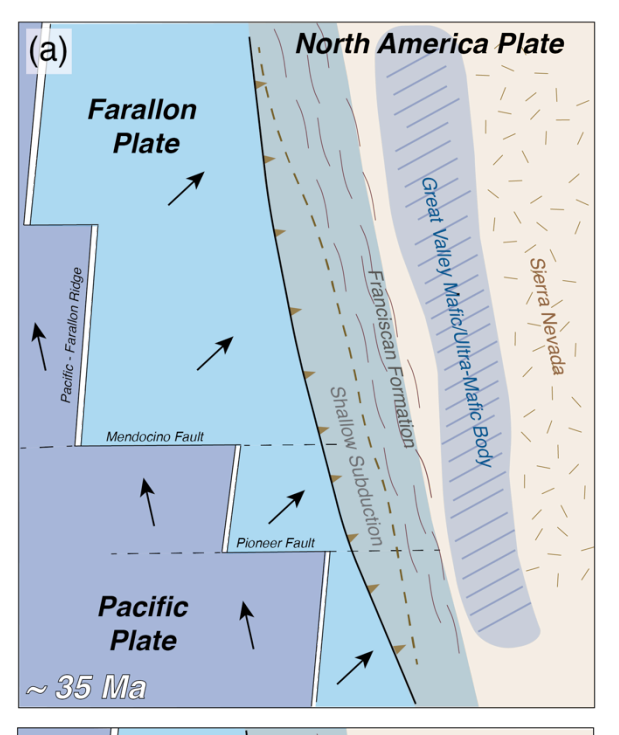
- McKenzie, K.A. & Furlong, K.P. (2021). Isolating non-subduction-driven tectonic processes in
- 891 Cascadia. Geoscience Letters, 8, 10. doi: <a href="https://doi.org/10.1186/s40562-021-00181-z">https://doi.org/10.1186/s40562-021-00181-z</a>
- McKenzie, K.A., Furlong, K.P., Herman, M.W. (2022). Regional and local patterns of upper-plate
- deformation in Cascadia: the importance of the down-dip extent of locking relative to upper-plate
- strength contrasts. Tectonics, (in press).
- McQuarrie, N., & Wernicke, B.P. (2005). An animated tectonic reconstruction of southwestern North
- 896 America since 36 Ma. Geosphere, 1(3), 147-172. doi: <a href="https://doi.org/10.1130/GES00016.1">https://doi.org/10.1130/GES00016.1</a>
- Melnick, D., Bookhagen, B., Echtler, H.P., & Strecker, M.R. (2006). Coastal deformation and great
- subduction earthquakes, Isla Santa Maria chile (37°S), GSA Bulletin, 118(11-12), 1463-1480. doi:
- 899 <u>https://doi.org/10.1130/B25865.1</u>
- 900 Meltzner, A.J., Sieh, K., Abrams, M., Agnew, D.C., Hudnut, K.W., Avouac, J.-P., & Natawidjaja
- 901 D.H. (2006). Uplift and subsidence associated with the great Aceh-Andaman earthquake of 2004.
- 902 JGR: Solid Earth, 111(B2). doi: https://doi.org/10.1029/2005JB003891
- 903 Muhs, D.R., Rockwell, T.K., & Kennedy, L. (1992). Late Quaternary Uplift Rates of Marine
- 904 Terraces on the Pacific Coast of North America, Southern Oregon to Baja California Sur. Quaternary
- 905 International, 15/16, 121-133. doi: https://doi.org/10.1016/1040-6182(92)90041-Y
- Rohr, K.M.M., Furlong, K.P., & Riedel, M. (2018). Initiation of Strike-Slip Faults, Serpentinization,
- and Methane: The Nootka Fault Zone, the Juan de Fuca-Explorer Plate Boundary. Geochemistry,
- 908 Geophysics, Geosystems, 19(11), 4290-4312. doi: <a href="https://doi.org/10.1029/2018GC007851">https://doi.org/10.1029/2018GC007851</a>
- Padgett, J.S., Kelsey, H.M., & Lamphear, D. (2019). Upper-plate deformation of Late Pleistocene
- marine terraces in the Trinidad, California, coastal area, southern Cascadia subduction zone.
- 911 Geosphere, 15(4), 1323-1341. doi: <a href="https://doi.org/10.1130/GES02032.1">https://doi.org/10.1130/GES02032.1</a>
- 912 Piotraschke, R., Cashman, S.M., Furlong, K.P., Kamp, P.J.J., Danišík, M., & Xu, G. (2015).
- 913 Unroofing the Klamaths Blame it on Siletzia? Lithosphere, 7 (4), 327-440. doi:
- 914 https://doi.org/10.1130/L418.1
- 915 Plattner, C., Malservisi, R., Furlong, F.P., & Govers, R. (2010). Development of the Eastern
- 916 California Shear Zone Walker Lane belt: The effects of microplate motion and pre-existing
- 917 weakness in the Basin and Range. Tectonophysics 485, 78–84.
- 918 doi: https://doi.org/10.1016/j.tecto.2009.11.021
- Ramírez-Herrera, M.T., Gaidzik, K., Forman, S., Kostoglodov, V., Bürgmann, R., & Johnson, C.W.
- 920 (2018). Relating the long-term and short-term vertical deformation across a transect of the forearc in
- 921 the central Mexican subduction zone, Geosphere, 14(2), 419-439. doi:
- 922 https://doi.org/10.1130/GES01446.1
- 923 Saillard, M., Audin, L., Rousset, B., Avouac, J.-P., Chlieh, M., Hall, S.R., Husson, L., & Farber, D.L.
- 924 (2017). From the seismic cycle to long-term deformation: linking seismic coupling and Quaternary
- oastal geomorphology along the Andean megathrust. Tectonics, 36(2), 241-256. doi:
- 926 https://doi.org/10.1002/2016TC004156

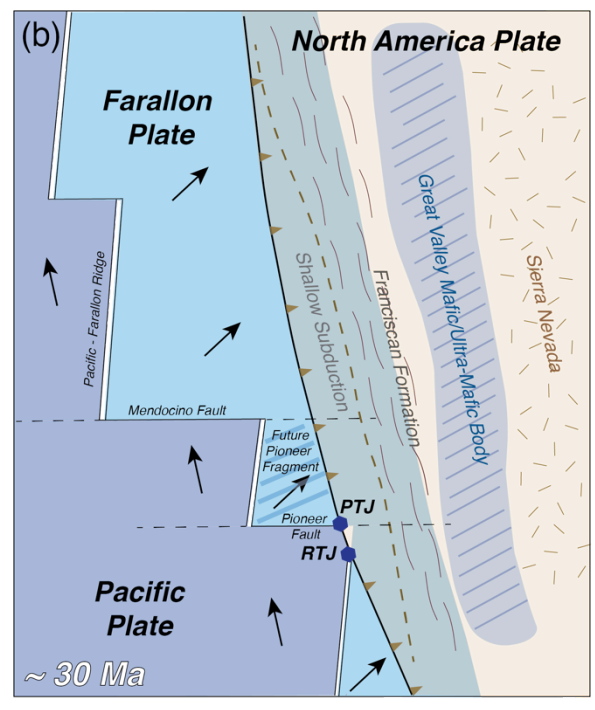
- 927 Savage, J.C., Svarc, J.L., Prescott, W.H., & Murray, M.H. (2000). Deformation across the forearc of
- 928 the Cascadia subduction zone at Cape Blanco. Oregon JGR: Solid Earth 105(B2), 3095–3102.
- 929 doi: https://doi.org/10.1029/1999JB900392
- 930 Schmalzle, G.M., McCaffrey, R., & Creager, K.C. (2014). Central Cascadia subduction zone creep.
- 931 Geochemistry, Geophysics, Geosystems, 15(4), 1515-1531. doi:
- 932 <u>https://doi.org/10.1002/2013GC005172</u>
- 933 Schmidt, W.L., & Platt, J.P. (2018). Subduction, accretion, and exhumation of coherent Franciscan
- blueschist-facies rocks, northern Coast Ranges, California. Lithosphere, 10(2), 301-326. doi:
- 935 https://doi.org/10.1130/L697.1
- 936 Schwanghart, W., & Scherler, D. (2014). TopoToolbox2 MATLAB-based software for topographic
- 937 analysis and modeling in Earth surface sciences. Earth Surface Dynamics, 2, 1-7. doi:
- 938 https://doi.org/10.5194/esurf-2-1-2014
- 939 Unruh, J., & & Humphrey, J. (2017). Seismogenic deformation between the Sierran microplate and
- 940 Oregon Coast block, California, USA. Geology, 45(5), 415-418. doi:
- 941 <u>https://doi.org/10.1130/G38696.1</u>
- 942 Unruh, J., Humphrey, J., & Barron, A., (2003). Transtentional model for the Sierra Nevada frontal
- fault system, eastern California. Geology, 31(4), 327-330. doi: https://doi.org/10.1130/0091-
- 944 7613(2003)031<0327:TMFTSN>2.0.CO;2
- Von Dassow, W., & Kirby, E. (2017). Geomorphic Evidence of Differential Rock Uplift Across the
- 946 Southern Cascadia Forearc. GSA Annual Meeting 2017, Seattle, Washington: Paper No. 247-12.
- 947 Geological Society of America Abstracts with Programs, v. 49, no. 6. doi:
- 948 https://doi.org/10.1130/abs/2017AM-307033
- 949 Wang, T., Wei, S., Shi, X., Oiu, O., Li, L., Peng, D., Weldon, R.J., & Barbot, S. (2018). The 2016
- 950 Kaikōura earthquake: Simultaneous rupture of the subduction interface and overlying faults. Earth
- and Planetary Science Letters, 482, 44-51, doi: https://doi.org/10.1016/j.epsl.2017.10.056
- Wells, R.E., Weaver, C.S., & Blakely, R.J. (1998). Fore-arc migration in Cascadia and its
- neotectonics significance, Geology, 26(8), 759-762. doi: https://doi.org/10.1130/0091-
- 954 7613(1998)026<0759:FAMICA>2.3.CO;2
- Whipple, K.X., & Tucker, G.E. (1999). Dynamics of the stream-power river incision model:
- 956 Implications for height limits of mountain ranges, landscape response timescales, and research needs.
- 957 JGR: Solid Earth, 104(B8), 17661-17674. doi: https://doi.org/10.1029/1999JB900120
- Wilson, D.S. (1993). Confidence intervals for motion and deformation of the Juan de Fuca Plate.
- 959 JGR Solid Earth 98(B9), 16053–16071. doi: https://doi.org/10.1029/93JB01227
- Wobus, C., Whipple, K.X., Kirby, E., Snyder, N., Johnson, J., Spyropolou, K., Crosby, B., &
- Sheehan, D. (2006). Tectonics from topography: Procedures, promise, and pitfalls. In Willett,
- 962 S.D., Hovius, N., Brandon, M.T., Fisher, D.M. (Eds.), Tectonics, Climate, and Landscape
- 963 Evolution, Geological Society of America Special Paper, vol. 398 (2006), pp. 55-74. doi:
- 964 <u>https://doi.org/10.1130/2006.2398(04)</u>

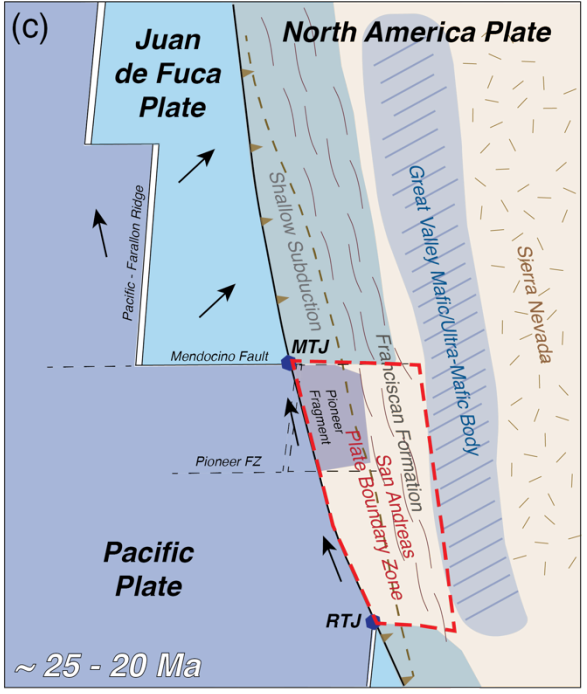
- 265 Zandt, G., & Furlong, K.P. (1982). Evolution and thickness of the lithosphere beneath coastal
- 966 California. Geology, 10(7), 376-381. doi: https://doi.org/10.1130/0091-
- 967 7613(1982)10<376:EATOTL>2.0.CO;2
- 268 Zandt, G., & Humphreys, E. (2008). Toroidal mantle flow through the western U.S. slab window.
- 969 Geology, 36(4), 295-298. doi: https://doi.org/10.1130/G24611A.1
- 970 13 Data Availability Statement
- 971 The GPS data used in this study are from the University of Nevada Reno's Geodetic Laboratory
- 972 (Blewitt et al. 2018) and can be accessed online: <a href="http://geodesy.unr.edu/">http://geodesy.unr.edu/</a>
- The benchmark leveling data plotted in Figure 7 are from Table 1 in Burgette et al. (2009) and can be
- 974 accessed online: <a href="https://doi.org/10.1029/2008JB005679">https://doi.org/10.1029/2008JB005679</a>
- The seismic tomography imagery shown in Figures 8 and 9 was produced by Antonio Villaseñor
- 976 (Institut de Ciències del Mar, Department of Marine Geosciences) and shared via a personal
- 977 communication.

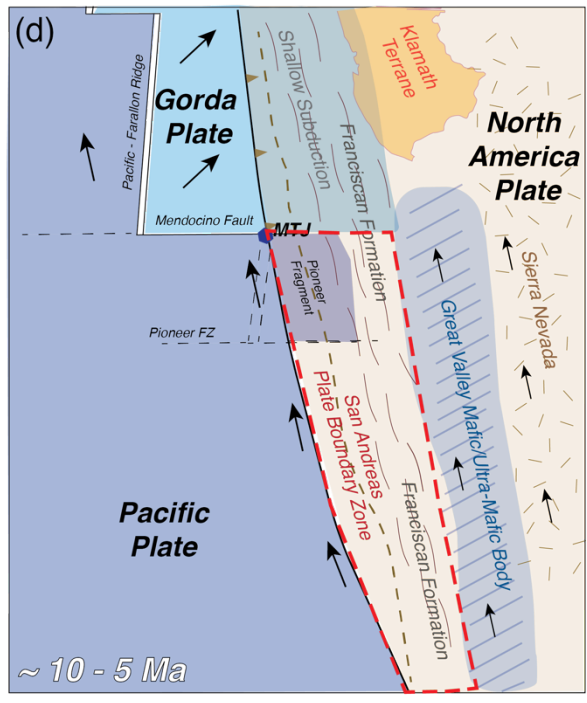


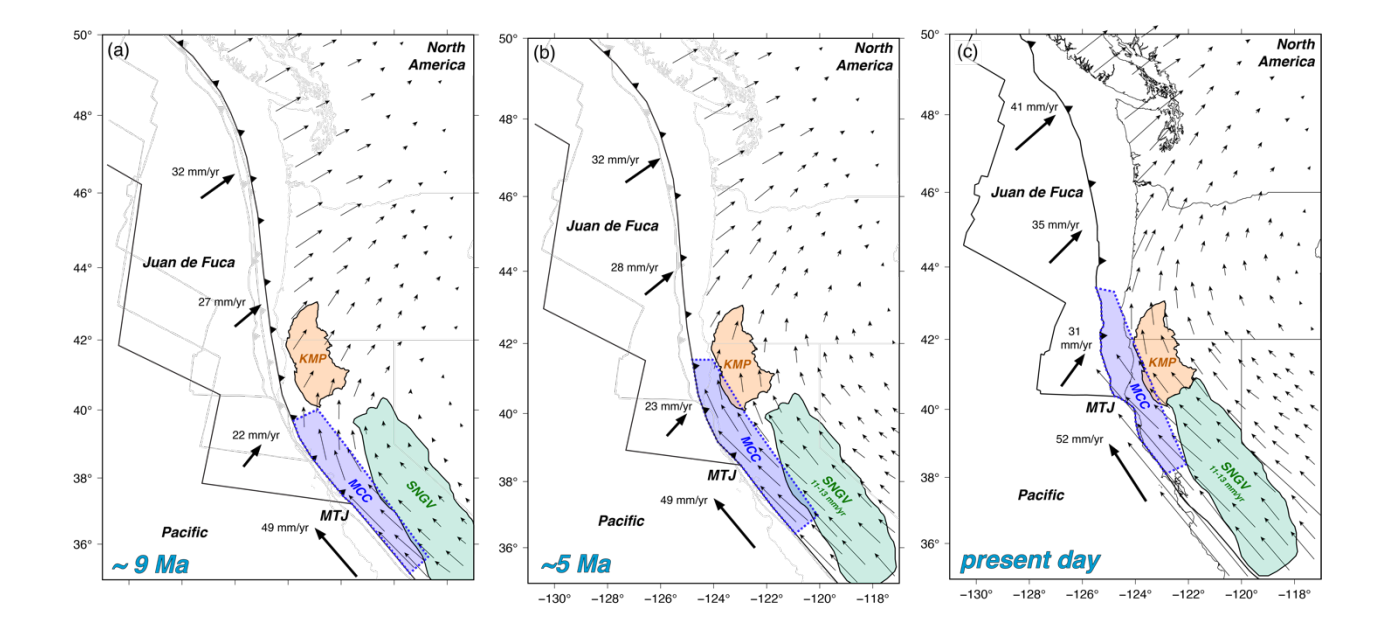


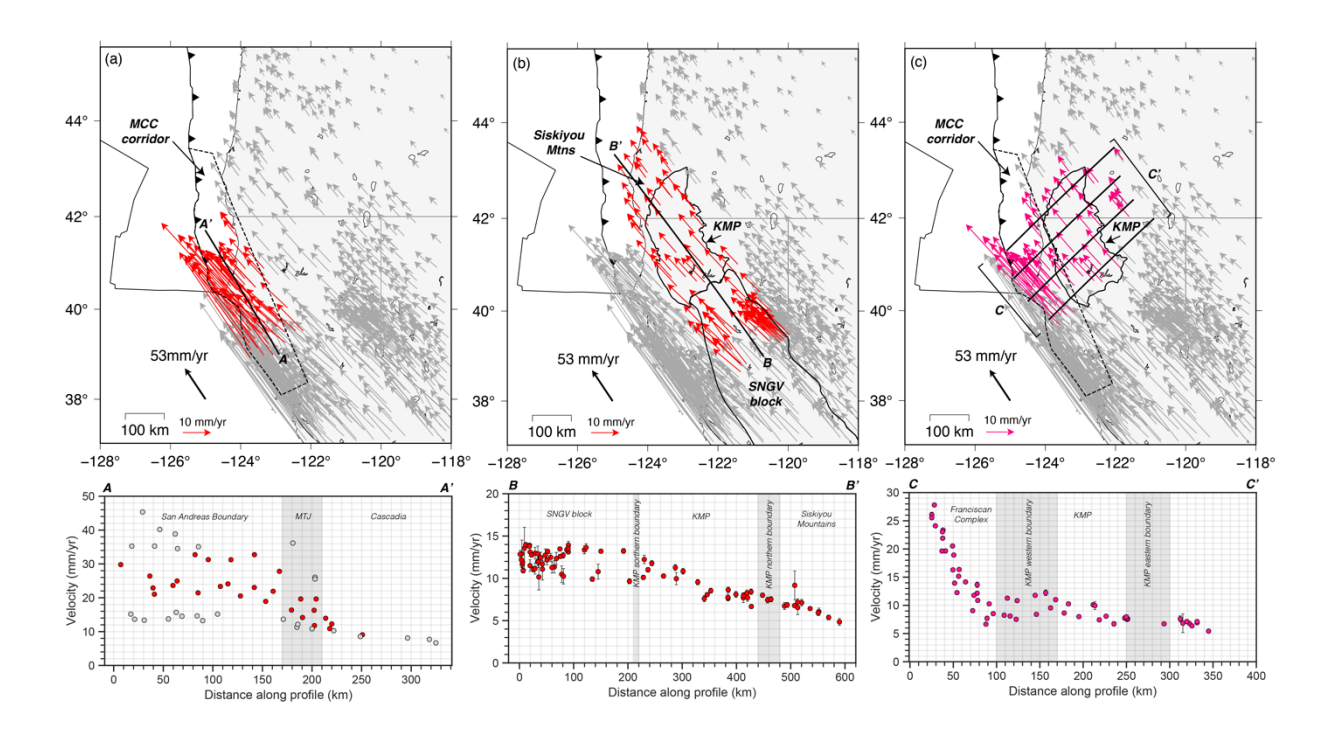


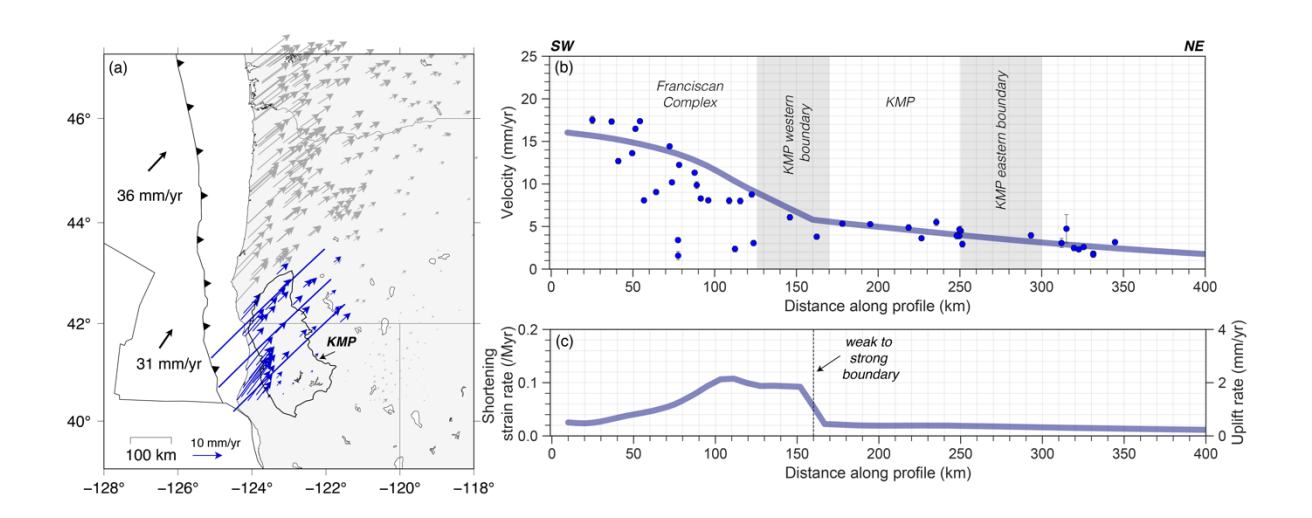


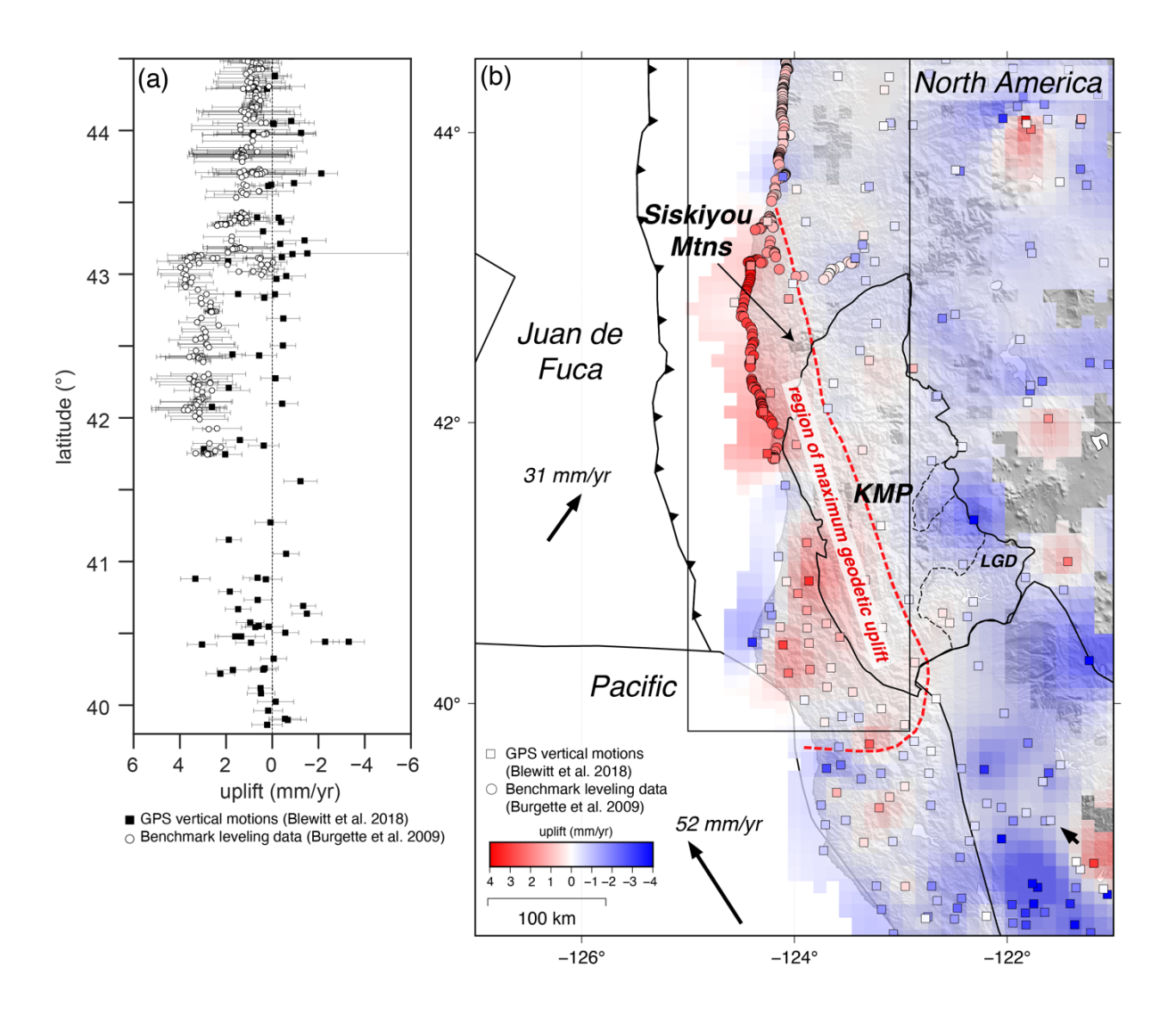


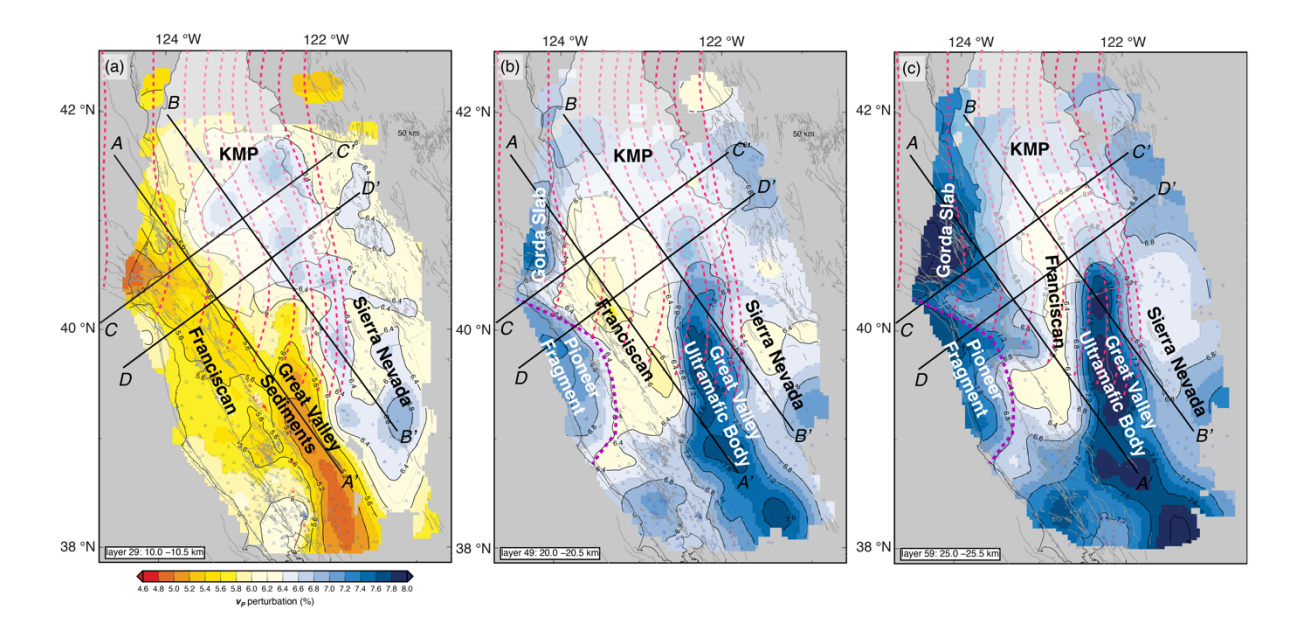


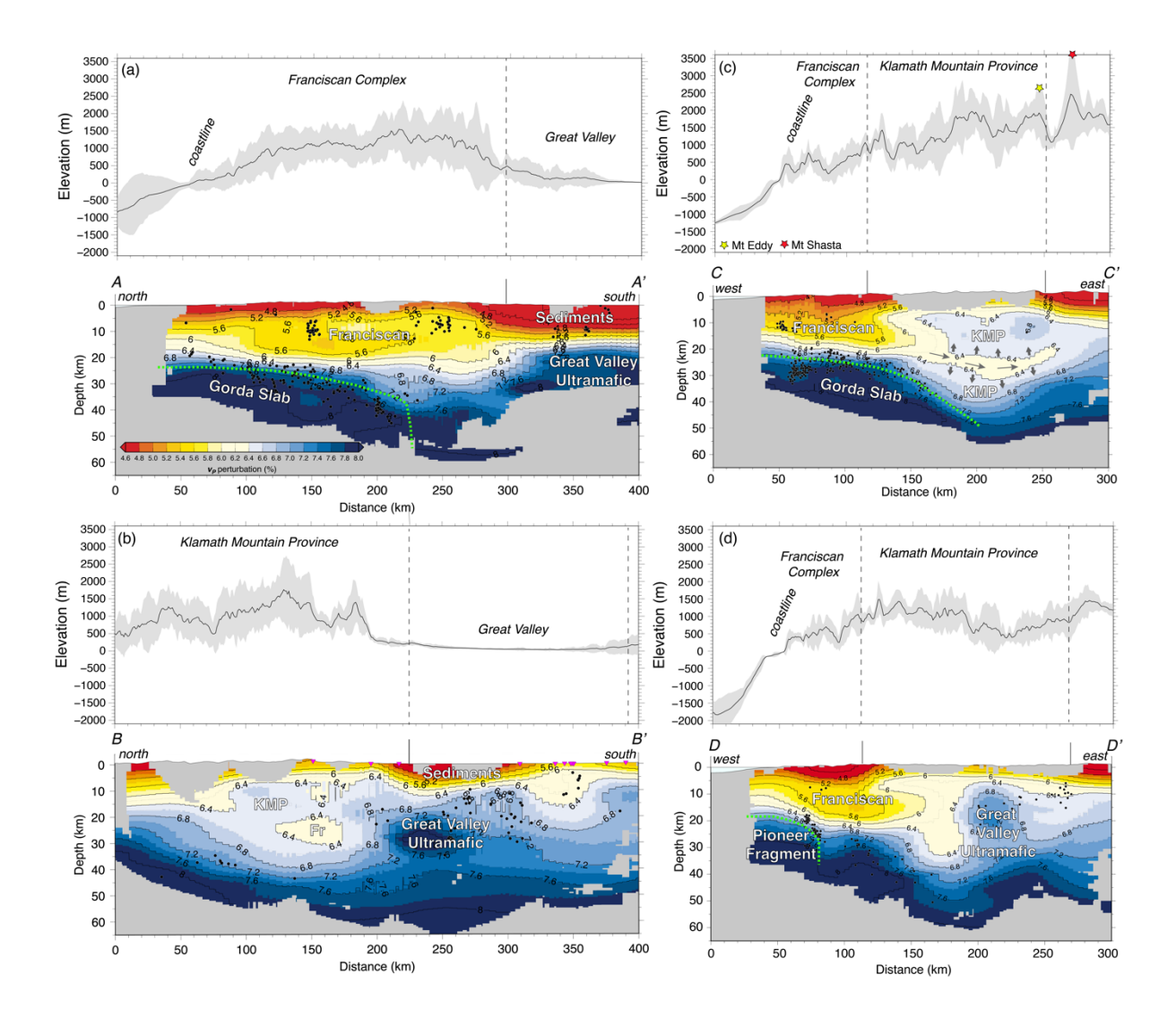


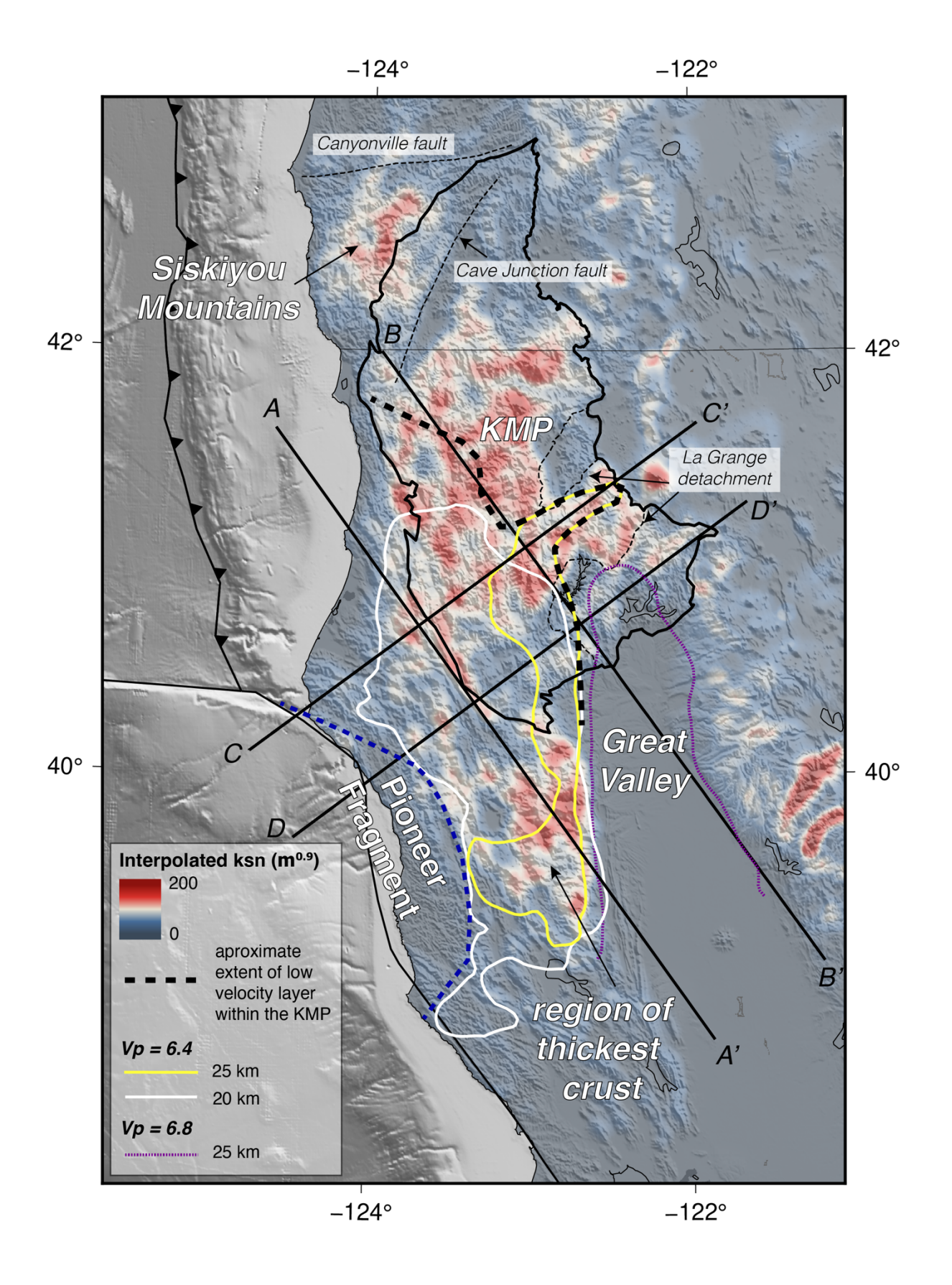


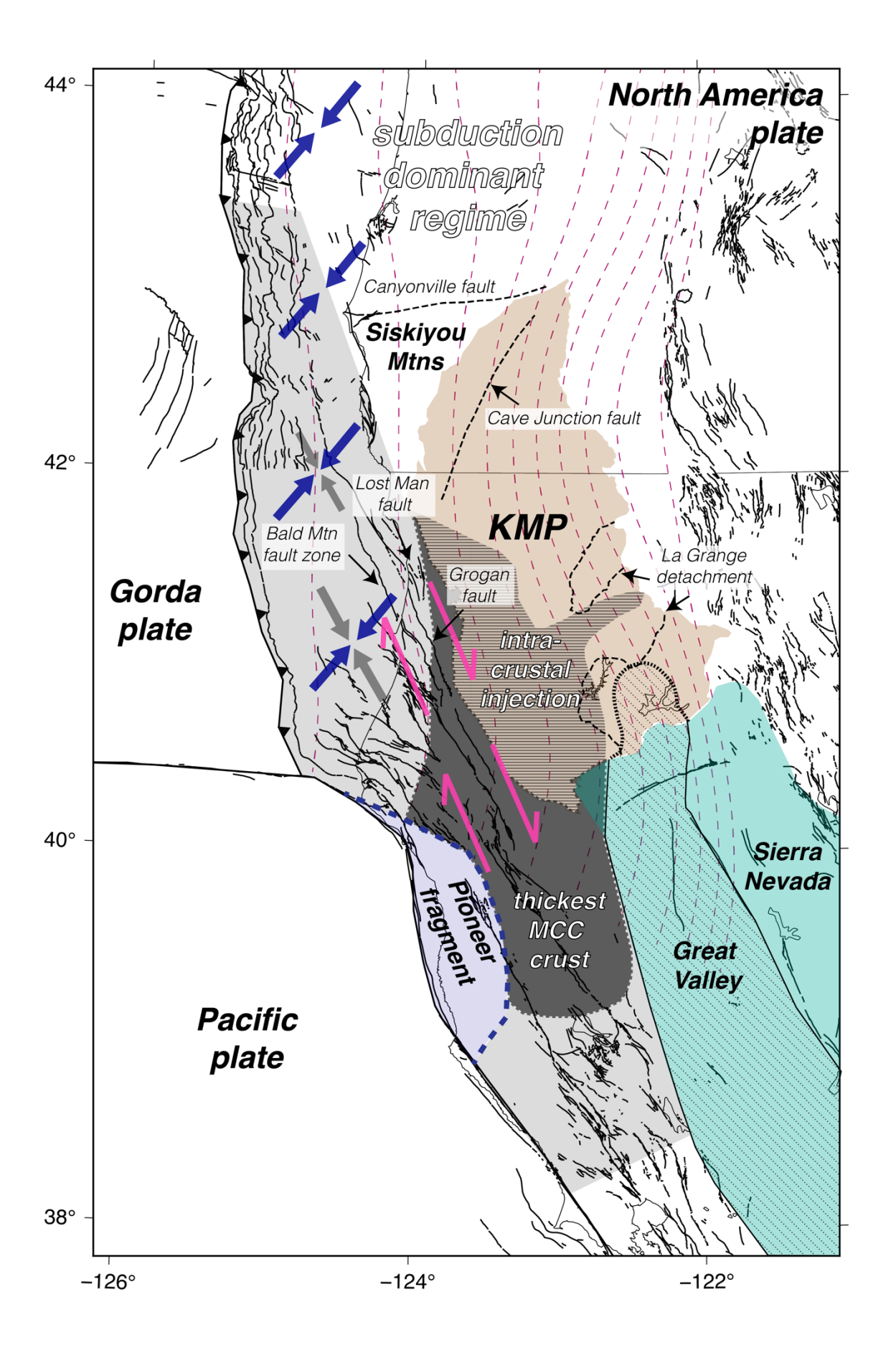












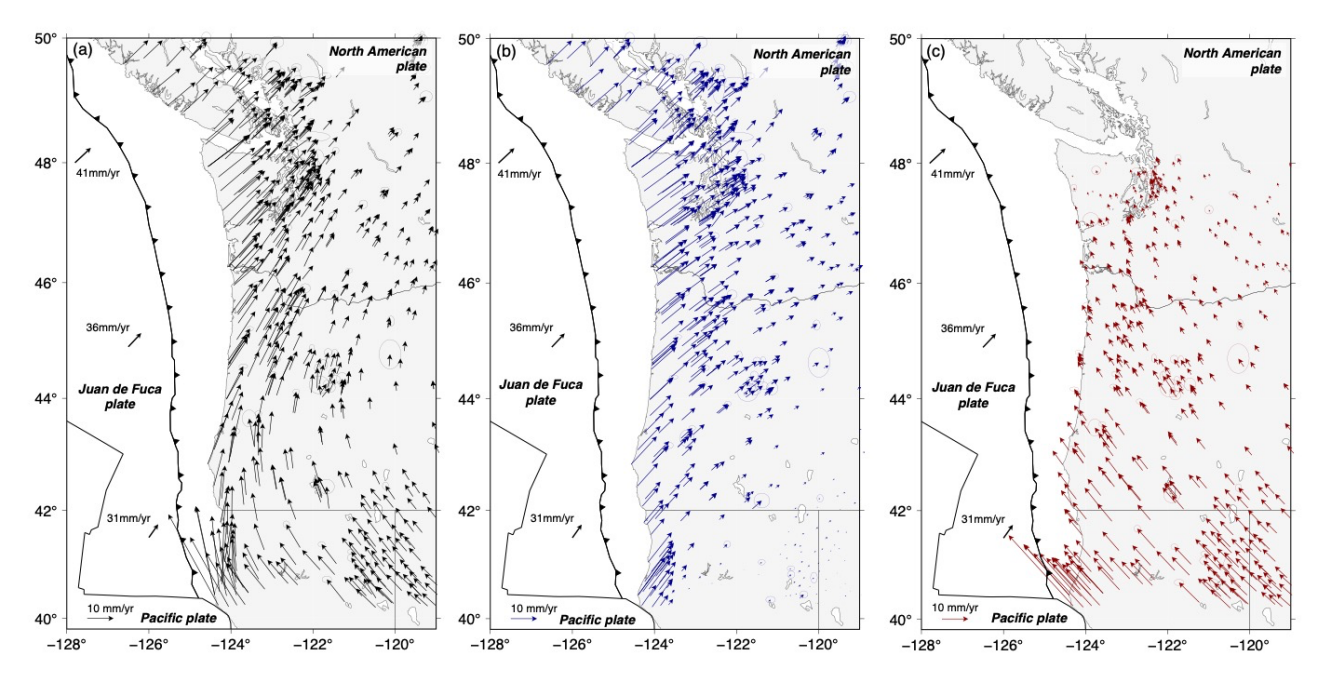


# Supplementary Material

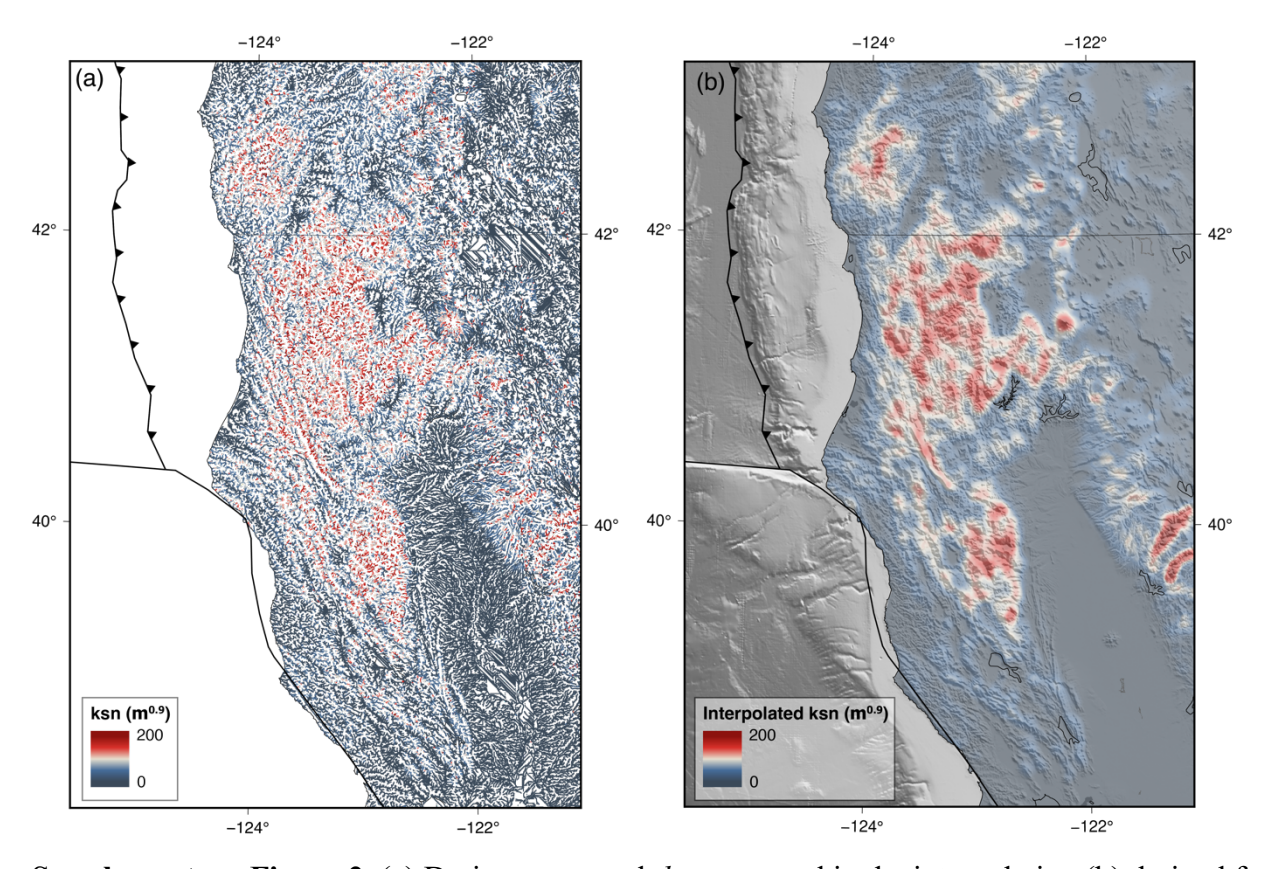
## 1 Supplementary Figures and Tables

This file includes supplemental figures S1, S2 & S3. Each are referenced in the main manuscript.

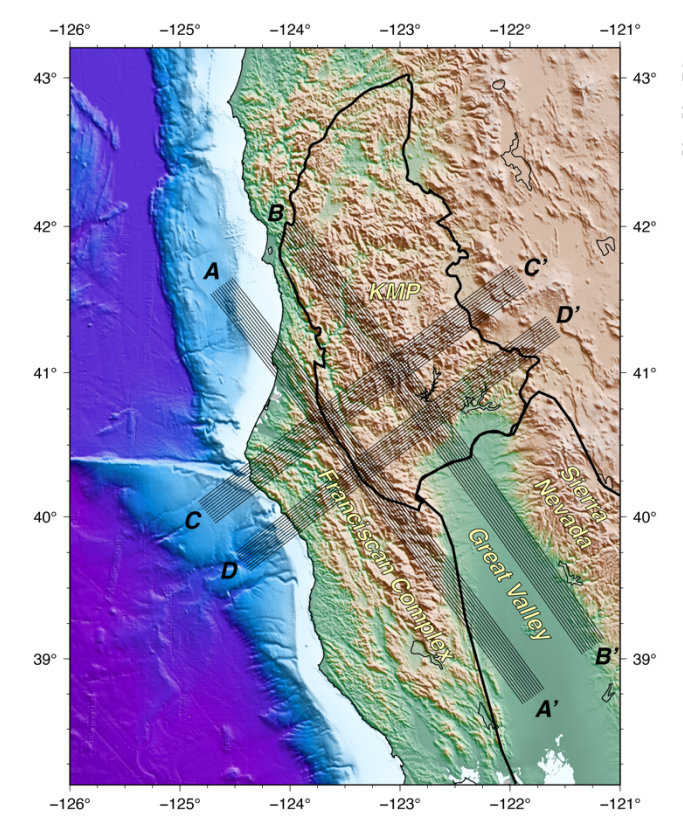
## 1.1 Supplementary Figures



**Supplementary Figure 1.** GPS velocity data, a subset of which are used in Figures 5 & 6. (a) GPS velocity data used in the GPS decomposition – GPS data are from the UNR Geodetic Laboratory. (b) Subduction (NE-directed, aligned with the Juan de Fuca-North America relative motion at each station) component of the GPS velocity field. (c) NNW-directed (aligned with the SNGV-North America relative motion at each station) GPS velocity field. The data shown in (a), (b), and (c) can be found in Supplementary Table 1.



**Supplementary Figure 2.** (a) Drainage network  $k_{sn}$  map used in the interpolation (b) derived from 30 m USGS DEM. Reference concavity = 0.45, smoothing distance = 1 km. (b) Interpolated  $k_{sn}$  map. Grid radius = 5 km.



**Supplementary Figure 3.** Map of study region showing the location of topographic swath profiles shown in Figure 9 in the main manuscript.